Quantifying Pathway Suitability for Fish Escaping Rapid Flow Changes

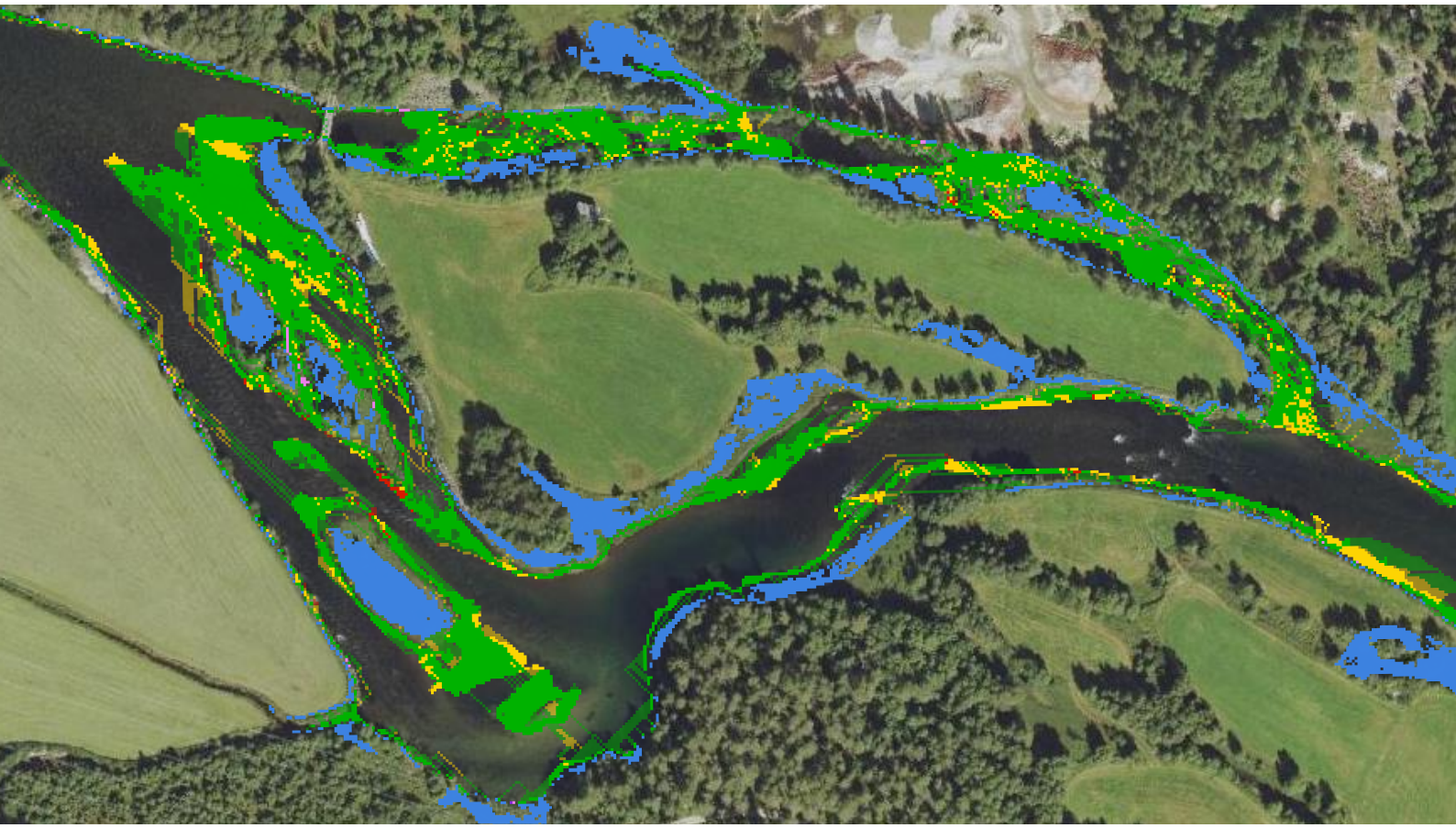

Master Thesis

Joël Ronald Wittmann

Chair: Prof. Dr. Roman Stocker (IfU)

Supervision: Dr. Luiz da Silva (IfU)
Dr. Davide Vanzo (VAW)

Date of submission: 12th of September 2022

Spring Semester 2022

IfU ETH zürich Environmental Microfluidics Group

Acknowledgement

I want to thank Professor Dr. Roman Stocker for supporting this Master Thesis. Furthermore, I thank Dr. Luiz da Silva and Dr. Davide Vanzo for their continuous support and technical assistance throughout this work. Together with Robert Naudascher the discussions during meetings proved very valuable.

Special thanks to Jan Baumgartner and Steffen Schweizer from Kraftwerke Oberhasli AG for providing both valuable feedback and data on the Hasliaare River. Also to Ana Juaréz, Dr. Ana Adeva-Bustos, Prof. Dr. Knut Alfredsen and Bjørn Otto Dønnum without whose data the validation would not have been possible.

Image title: Escape routes in the Storåne River at Hovet (Norway), Kartverket, 2022

Abstract

Hydropower electricity production is expected to further increase over the next decades as part of climate change mitigation. Fish stranding and drifting ensue from associated hydropeaking potentially threatening population stability. The dewatering rate is commonly used to characterise stranding risk but neglects the influence of bed topography. The previously developed raster based Fish Escaping Routes (FiER) model estimates optimum routes for fish escaping habitats becoming unfavourable during hydropeaking. It was extended to quantify the route suitability: Along the optimum escape routes required swimming speeds are estimated and suitability is determined by comparison with fish swimming capacities. New indicators were defined aggregating the spatially distributed results. The model was subjected to a sensitivity analysis and validation showing promising first results. Application of the model on various study sites illustrates the potential of the model for both river management and research. During application a net benefit of higher morphological complexity for persistent fish habitat is indicated although route suitability decreases. Further development of the model should focus on extending the validation and incorporating actual fish behaviour.

Die Stromproduktion durch Wasserkraft als wichtiger Beitrag zur Bekämpfung des Klimawandels wird in den nächsten Jahrzehnten voraussichtlich zunehmen. Schwall und Sunk als Folge der Wasserkraftnutzung verursachen Stranden und Verdriften von Fischen und gefährden damit potentiell den Erhalt stabiler Populationen. Die Pegelrückgangsrate wird vielfach verwendet um das Strandungsrisiko abzuschätzen, vernachlässigt jedoch den Einfluss der Gewässersohle. Das bereits zuvor entwickelte, rasterbasierte Fish Escaping Routes (FiER) Modell bestimmt optimale Fluchtrouten für Fische, welche aus Habitaten fliehen, die während Abflussänderungen ungeeignet werden. Das Modell wurde erweitert, um die Eignung der Routen zu quantifizieren: Hierzu werden entlang der optimalen Fluchtwege die benötigte Schwimmgeschwindigkeit berechnet und durch ein Vergleich mit der Schwimmfähigkeit die Eignung bestimmt. Neue Indikatoren wurden definiert, um die räumlich verteilten Ergebnisse zu aggregieren. Eine Sensitivitätsanalyse und Validierung des Modells liefern vielversprechende erste Resultate. Das Potential des FiER Modells wurde an verschiedenen Versuchsstrecken aufgezeigt. Eine komplexere Gewässermorphologie zeichnet sich als effektiv geeigneteres Fischhabitat ab, obwohl deren Fluchtwege weniger geeignet sind. Die weitere Entwicklung des Modells sollte sich verstärkt mit der Validierung und dem tatsächlichen Verhalten der Fische auseinandersetzen.

Contents

1. Introduction

Modern human life leaves a mark on our planet. Steffen et al., 2015 visualise with their planetary boundaries the increasingly evident possibility of humanity irreversibly perturbing the earth system. Climate change gained rapidly increasing attention over the last decades and receives most of the international effort regarding the nine planetary boundaries in Figure 1 (Chan, Stavins and Ji, 2018). To reach the goals of the Paris Agreement CO_2 emissions from electricity production must be reduced to zero (IPCC, 2022). Hydropower is expected to play an important role in climate change mitigation providing low-emission electricity production and storage capacity (IPCC, 2011; Berga, 2016; s. Box 1). Hydropower plants, however, also create adverse environmental impacts putting additional stress on biosphere integrity - another planetary boundary which is already at high risk (Figure 1). With an expected increase in hydropower production minimising the impacts is essential (IPCC, 2011; Zarfl et al., 2015). On national and international level efforts are made focusing on, among others, fish stranding from hydropeaking (Killingtveit, 2018; Tonolla et al., 2017; WPO, 2021). Stranding occurs when falling water levels leave fish trapped in disconnected parts of the river (pool stranding) or in sediment interstices (interstitial stranding) (Larrieu, Pasternack and Schwindt, 2021). With thousands of fish reportedly affected in a single event hydropeaking on daily or sub-daily frequency potentially threatens population stability (Higgins and Bradford, 1996; Greimel et al., 2018; Larrieu, Pasternack and Schwindt, 2021). It is more pronounced in morphological complex river reaches otherwise desirable for providing fish habitat (Nagrodski et al., 2012; Vanzo, Guido and Siviglia, 2015; Lüthy et al., unpub.). As with hydropower itself mitigation of its consequences, therefore, contains a conflict of goals asking for optimised solutions.

Figure 1: Planetary boundaries & their status. By J. Lokrantz/Azote based on Steffen et al., 2015.

An often used indicator for stranding risk is the dewatering rate, i.e. the decrease in water surface elevation per time interval (Tonolla et al., 2017; Juárez et al., 2019). Experimental studies, however, report varying results on its relevance for stranding (supporting: Auer et al., 2017; Irvine et al., 2009; Halleraker et al., 2003; Michael Bradford et al., 1995, opposing: Michael Bradford, 1997; Bell et al., 2008). The differences might be partially explained by variations in bed topography which can, as illustrated in Figure 2, lead to longer escape movement routes at the same dewatering rate. Addressing this effect, Lüthy et al., unpub. developed the Fish Escaping Routes (FiER) model

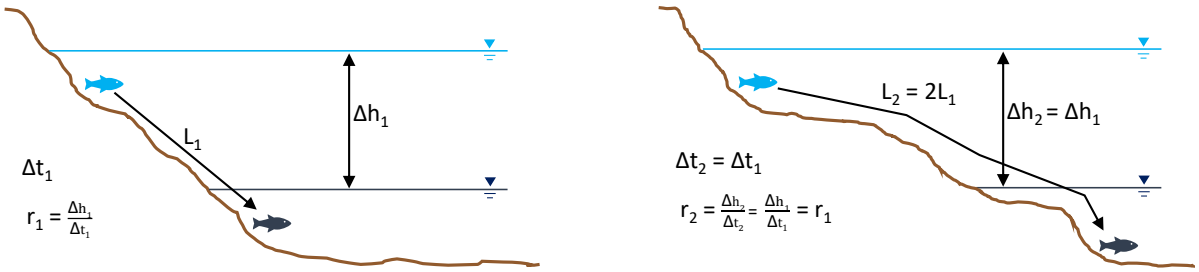

(a) Short path (b) Long path

Figure 2: Both scenarios feature the same dewatering rate r, although the path a fish has to migrate in case (a) is only half the length L as in case (b).

to estimate the path length of optimum fish escape movement. This Thesis continues the development of the model by evaluating the capability of fish species to follow the optimum routes. Hence, it enables the quantification of the stranding as well as the drifting risk (s. Box 1). Furthermore, the Thesis tests parameter sensitivities, validates the model and proposes indicators to allow a comparison between different reaches and hydropeaking scenarios. Finally, two potential application areas, research and river management, are outlined by one case study each.

Box 1: General Terminology

Hydropower: Conversion of energy from flowing water (kinetic) into another form, mostly electricity using turbines. Flexibility of power production, environmental impacts and storage capacities vary with the type of power plant. (IPCC, 2011)

Fish stranding: Trapping of fish by falling water levels either in disconnected river parts (pool stranding) or in sediment interstices (interstitial stranding). (Larrieu, Pasternack and Schwindt, 2021)

Fish drift: Displacement of fish by a current where they have only limited control over their movement. Drift may be entered on purpose (active drift) or accidentally (passive drift). (Lechner, Keckeis and Humphries, 2016)

Hydropeaking: Discontinuous release of water from a reservoir, e.g. for hydropower, causing an increase (upramping) or decrease (downramping) in water level. (Greimel et al., 2018)

Fish habitat: Area in a river preferred by fish for successful survival and reproduction, usually defined by physical parameters (e.g. depth, velocity). Preferred conditions vary with species and life stages. (Melcher, Hauer and Zeiringer, 2018)

Escape movement: Directed movement of an organism to escape from unfavourable conditions. Changes in river flow, e.g. from hydropeaking, can turn previously suitable habitats unfavourable triggering escape movement. (Lucas et al., 2001)

2. Methodology

The methodology is separated into two parts, first describing the FiER model in Section 2.1. Afterwards, the model was applied on different study reaches as described in Section 2.2.

2.1. Fish Escaping Routes Model

The FiER model estimates the capability of fish to move with shifting habitats, e.g. under hydropeaking conditions. It is written in Java and requires raster input data as Tagged Image File Format (TIFF) for water depth, flow velocity in x- and y-direction, and binary habitat suitability, usually obtained from a 2D steady state hydrodynamic model, together termed *input raster set*. Habitat shift is represented by a sequence of input raster sets with a specified duration between them, for instance corresponding to increasing discharge in an upramping scenario. Additionally, swimming capacities and preference curves for the considered fish species are required.

In between the specified habitats of two consecutive input raster sets a path finding algorithm determines the optimum path a fish could take (Section 2.1.1). Afterwards, a second algorithm calculates the velocity a fish must exert to successfully complete the obtained path (Section 2.1.2). Finally, indicators are derived in Section 2.1.3 assessing the capability of the fish to move with the shifting habitat.

The model structure and indicator behaviour is studied with a sensitivity analysis in Section 2.1.4. A validation is conducted to estimate the model performance in Section 2.1.5.

2.1.1. Path Calculation

The path finding algorithm is identical to the Flow Field Approach in Lüthy et al., unpub. from whom the code was received. Only small adjustments regarding data handling to facilitate the indicator calculation were made. This section explains the essential parts of their algorithm used in the model, for further details see Lüthy et al., unpub.

The algorithm, illustrated in Figure 3, starts in one of the cells labelled as habitat in the first input raster set. This cell is called *origin*. Using a modified Dijkstra algorithm it calculates the optimum route to any cell marked as habitat in the next input raster set (*target*). The obtained route between the two input raster sets is termed *path segment*. Iterating over all cells marked as habitat in the first input raster set yields one path segment per origin. The procedure is repeated for all consecutive pairs of input raster sets which are termed *discharge increments* ΔQ. A sequence of path segments across all discharge increments forms the *total path* of an origin. Box 2 summarises the defined terms.

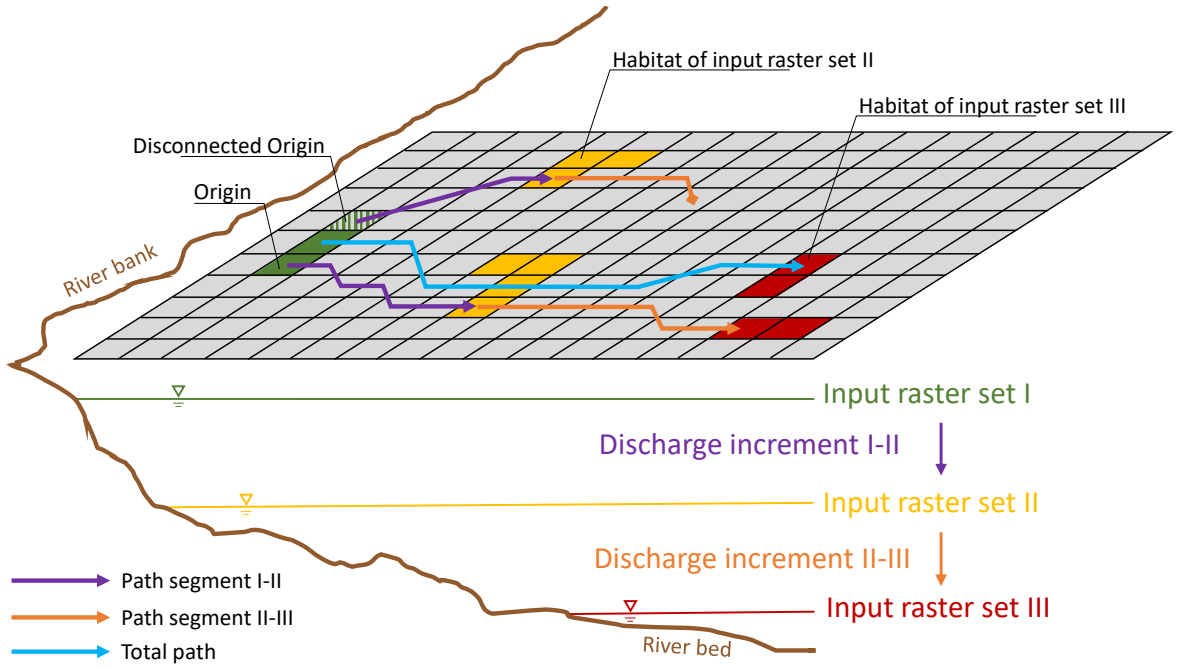

Figure 3: For each origin cell (green), the optimum path segment (purple) to any habitat cell of the second input raster set (yellow) is computed. The path is continued (orange) to any of the habitat cells in the third input raster set (red). The total path (blue) of a origin is formed by its path segments. If a path segment cannot reach a target, the corresponding origin cell is rendered disconnected.

Box 2: Model Terminology

Input raster set: Ensemble of suitability, depth, x- and y-velocity raster of the same discharge.

Hydraulic scenario: An ordered sequence of input raster sets describing the hydraulics during hydropeaking.

Discharge increment ΔQ: Two input raster sets of consecutive discharges. They represent one step of the hydraulic scenario and correspond to one model iteration.

Origins: Cells labelled as suitable in the first input raster set of the hydraulic scenario. They form the suitable fish habitat prior to the hydropeaking event.

Source: Cells labelled as suitable in the first input raster set of the current discharge increment. Current path-finding starts from these cells if they were reached during the previous iteration.

Target: Cells labelled as suitable in the second input raster set of the current discharge increment. Current path-finding tries to reach these cells.

Path segment: The computed optimum escape route between the source and target cells of a discharge increment.

Total path: An ordered sequence of path segments forming the escape route from an origin cell to any target cell of the last input raster set of the hydraulic scenario.

Result image: Rendered image visualising origins, targets and paths within the river reach.

Modified Dijkstra Algorithm

Starting from the origin cell currently considered (*source*) the modified Dijkstra algorithm calculates and stores the movement cost to each valid neighbouring cell (Figure 4.1). A neighbouring cell is viable if it is horizontally, vertically or diagonally adjacent, not outside the model boundaries and if water depth is larger than a specified minimum (Figure 4.2). The neighbour with the lowest movement cost is selected next (Figure 4.3) and the movement cost to its viable neighbours calculated (Figure 4.4). Adding to those the cost already incurred by moving from the origin to the selected neighbour gives the total cost to reach these cells from the origin (Figure 4.5). Next, the algorithm moves to the cell with the lowest cost not previously selected (Figure 4.6). If total movement costs for a neighbour were calculated before, they are updated in case lower total costs are obtained in the current iteration (Figure 4.7). This process is repeated until one of the target cells is reached (Figure 4.8). To potentially find cheaper paths the algorithm continues the iteration until either

a) all not previously selected cells have a higher cost assigned than the target,

b) all not previously selected cells exceed a specified cost threshold or

c) all reachable cells have been selected.

Condition a) and b) reduce computational time whereas b) and c) can result in no path being found which turns the origin cell to a dead end. It is stored as such and treated as disconnected during indicator calculation (Section 2.1.3). In a last step the path segment is constructed via backtracking from the target cell. After termination the algorithm is restarted with the next origin point as source cell. When all origin points have been considered the model moves to the next discharge increment transferring all target cells reached by a path segment as the new set of source cells.

Cost Calculation

Calculation of the movement costs for the modified Dijkstra algorithm considers the movement angle against the flow and the absolute flow velocity. A dynamic exponential function, illustrated in Figure 5, describes the movement probability per angle (Equation 1). The movement angle against the flow is discretised into eight intervals. Depending on the absolute flow velocity the shape of the function is adjusted through a λ-factor. The movement probability $f_\lambda(x)$ is normalised in Equation 2. Finally, Equation 3 translates the normalised probability into movement costs.

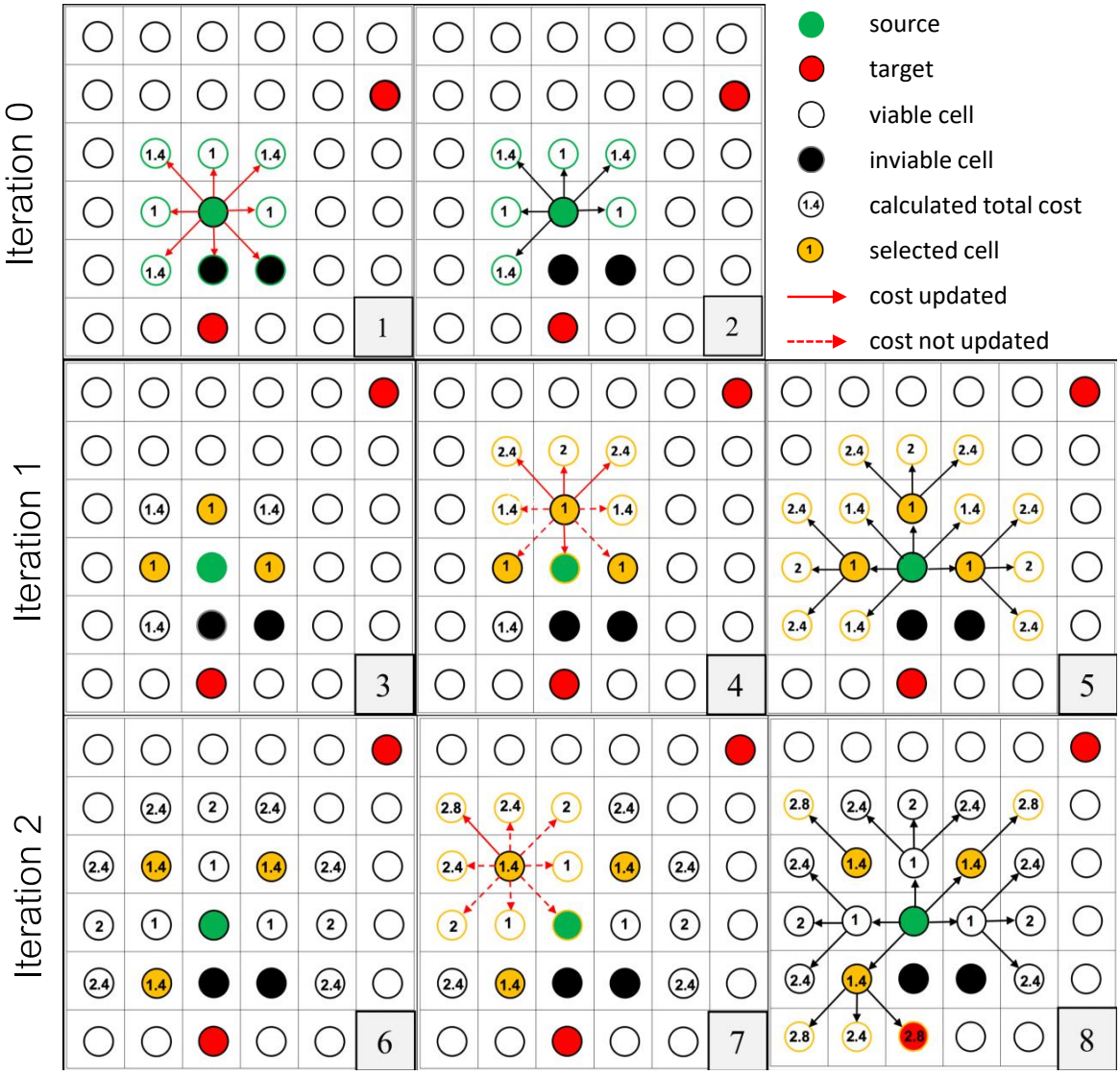

Figure 4: Illustration of the modified Dijkstra algorithm. During iteration 0 the cost, here equal to the distance, of viable neighbours is calculated (1) & (2). In the subsequent iteration 1 cells with the lowest cost are selected (3) and the cost of their potentially neighbours updated (4) resulting in an expanded cost field (5). The process is repeated for the next highest cost (6) & (7) until the target is reached (8). The algorithm continues to iterate until all not previously selected cells have a higher cost than the target (not illustrated). Adapted from Lüthy et al., unpub.

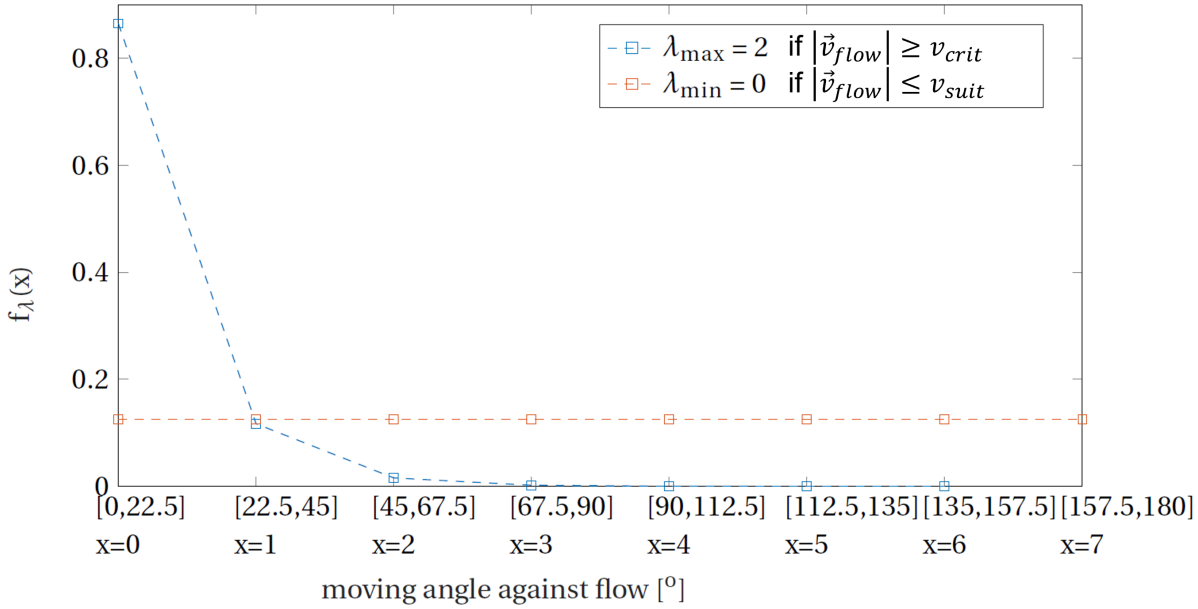

Figure 5: Movement probability $f_\lambda(x)$ per discretised flow angle x. Movement with the flow corresponds to $x = 0$, against the flow to $x = 7$. The shape of $f_\lambda(x)$ is adjusted for the flow velocity by λ (Equation 1). From Lüthy et al., unpub.

$$f_\lambda(x) = \lambda e^{-\lambda x} \qquad (1)$$

$$f_{\lambda,norm.}(x) = \frac{f_\lambda(x)}{\sum_{x=0}^{7} f_\lambda(x)} \qquad (2)$$

$$c_{i \to i+1} = \frac{1}{f_{\lambda,norm.}(x)} \qquad (3)$$

where

$f_\lambda(x)$	Probability function [−]
$x \in [0, 7]$	Discretised angle against flow [−]
$f_{\lambda,norm.}(x)$	Normalised probability function [−]
λ	Absolute flow velocity factor [−]
$c_{i \to i+1}$	Movement cost to neighbour [−]

At low flow velocities, i.e. up to the suitable velocity v_{suit} of the considered fish species, the movement angle against the flow is assumed to be irrelevant, corresponding to $\lambda_{min} = 0$. Consequently, the cost is the same in all directions and the dynamic exponential function collapses into a horizontal line (Figure 5). For absolute flow velocities exceeding the critical velocity v_{crit} of the fish species λ_{max} is fixed to 2, i.e. to an 86% probability for movement with the flow. These values give reasonable results but are not based on scientific studies. However, λ_{max} can be adjusted by the modeller. In between λ is linearly interpolated adjusting the exponential function accordingly. Setting an intermediate point for the interpolation, i.e. defining λ_{mid} at v_{mid}, gives more control over the dynamic behaviour. Naturally, two constrains for the six parameters arise:

$$v_{suit} \leq v_{mid} \leq v_{crit} \qquad \lambda_{min} \leq \lambda_{mid} \leq \lambda_{max}$$

2.1.2. Pathway Suitability

When following the paths estimated in section 2.1.1, fish are exposed to currents. Although flow velocity is considered during the path-finding algorithm it may still provide paths through currents too strong for the fish species. The capability of the fish to overcome them is not yet assessed. Flow velocities exceeding the swimming capacity result in passive drift preventing the fish from reaching its target habitat (Lechner, Keckeis and Humphries, 2016). Hence, the FiER model was extended to also consider fish velocities. The velocity a fish must exert to follow the optimum path, $|\vec{v}_{fish}|$, is governed by

1. the required speed along the path to reach the next habitat in time, $\vec{v}_{path}$,

2. and the flow velocity at the current location of the fish, $\vec{v}_{flow}$.

Path velocity $\vec{v}_{path}$ is computed for each path segment (Equation 4). It is defined as the velocity the fish has to swim on average, to complete the current path segment just within the duration of the corresponding ΔQ. Flow velocity $\vec{v}_{flow}$ is defined per cell and ΔQ (equation 5) and obtained from the provided velocity rasters (s. Section 2.1.1).

$$\vec{v}_{path,k} = \frac{L_{Path,k}}{\Delta t_k} * \hat{\vec{p}} \qquad (4)$$

$$\vec{v}_{flow,k} = \begin{pmatrix} v_{x,k} \\ v_{y,k} \end{pmatrix} \qquad (5)$$

where

k	Current discharge increment index $[-]$	$L_{Path,k}$	Path segment length $[m]$
Δt_k	Duration of discharge increment k $[s]$	$\hat{\vec{p}}$	Unit vector in path direction $[-]$
v_x	Flow velocity x-direction $\left[\frac{m}{s}\right]$	v_y	Flow velocity y-direction $\left[\frac{m}{s}\right]$

Since $\vec{v}_{flow}$ does not necessarily coincide with the direction of $\vec{v}_{path}$, as illustrated in Figure 6, the fish may need to adjust its movement direction by swimming $\vec{v}_{fish}$. Adding

$$\vec{v}_{eff} = \vec{v}_{flow} + \vec{v}_{fish} \qquad (6)$$

gives the effective movement $\vec{v}_{eff}$ of the fish. To reach the end of the path in time, $\vec{v}_{eff}$ also has to be equal to or larger than $\vec{v}_{path}$. $\vec{v}_{fish}$ is defined as the shortest vector satisfying both criteria:

$$\vec{v}_{eff} \parallel \vec{v}_{path} \qquad |\vec{v}_{eff}| \geq |\vec{v}_{path}|$$

The shortest vector $\vec{v}_{fish}$ satisfying $\vec{v}_{eff} \parallel \vec{v}_{path}$ is perpendicular to $\vec{v}_{path}$ through $\vec{v}_{flow}$ (s. Figure 6a). Its resulting $\vec{v}_{eff}$ can be described by $\vec{v}'_{flow}$, i.e. the projection of $\vec{v}_{flow}$ on $\vec{v}_{path}$. The second criteria is satisfied as well, if $\left|\vec{v}'_{flow}\right| \geq |\vec{v}_{path}|$. In this case the fish needs to only adjust its movement direction and $|\vec{v}_{fish}|$ can be calculated as

$$|\vec{v}_{fish}| = \left| \frac{\vec{v}_{flow} \cdot \vec{v}_{path}}{|\vec{v}_{path}|^2} * \vec{v}_{path} - \vec{v}_{flow} \right| \qquad (7)$$

If $\left|\vec{v}'_{flow}\right| < |\vec{v}_{path}|$ adjusting only the movement direction will yield a too slow effective movement of the fish, i.e. the fish does not reach the end of the path in time. In case $\left|\vec{v}'_{flow}\right| < 0$ it would move in the wrong direction (s. figure 6b). Consequently, the fish needs to additionally accelerate itself in the direction of $\vec{v}_{path}$. Hence, the shortest $\vec{v}_{fish}$ results in $\vec{v}_{eff} = \vec{v}_{path}$, allowing to rearrange Equation 6 into

$$|\vec{v}_{fish}| = |\vec{v}_{path} - \vec{v}_{flow}| \tag{8}$$

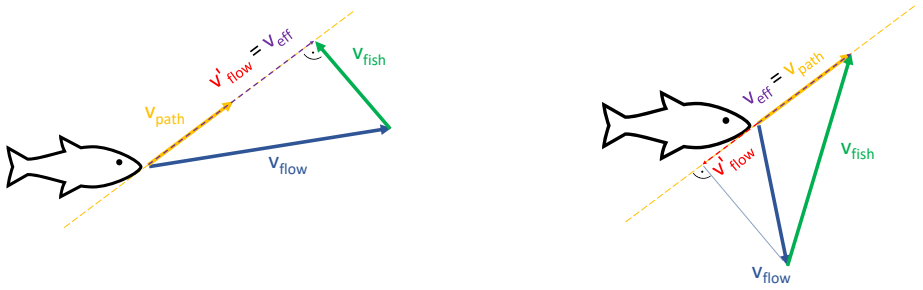

(a) $\left|\vec{v}'_{flow}\right| \geq |\vec{v}_{path}|$ (b) $\left|\vec{v}'_{flow}\right| < |\vec{v}_{path}|$

Figure 6: Definition of $\vec{v}_{fish}$ begins with the projection of $\vec{v}_{flow}$ on $\vec{v}_{path}$, yielding two cases: (a) $\left|\vec{v}'_{flow}\right|$ is larger or equal to $|\vec{v}_{path}|$. The fish needs to adjust only its movement direction. (b) the projected flow velocity $\left|\vec{v}'_{flow}\right|$ is smaller than $|\vec{v}_{path}|$. The fish needs to adjust its movement direction and speed.

Calculation of $|\vec{v}_{fish}|$ is performed for each cell along a path. Comparing $|\vec{v}_{fish}|$ to the swimming capacities of the considered fish species gives the capability of the fish to follow the path defining three categories of pathway suitability (Table 1). Fish are considered incapable of following paths containing one or more cells of supercritical $|\vec{v}_{fish}|$. Accordingly, source and target habitat connected by this path are termed disconnected.

Comparison	Fish Velocity	Assumed Connectivity
$\|\vec{v}_{fish}\| \leq v_{suit}$	suitable	connected
$v_{suit} < \|\vec{v}_{fish}\| \leq v_{crit}$	subcritical	connected
$v_{crit} < \|\vec{v}_{fish}\|$	supercritical	disconnected

Table 1: Fish velocity $|\vec{v}_{fish}|$ is divided in three categories by comparison with the suitable velocity v_{suit} and the critical velocity v_{crit} of the considered fish species.

Computation of $|\vec{v}_{fish}|$ as described above was implemented in the Java code along with adaptions to the user interface for providing required parameters. Additionally, the result image, showing habitats and paths in the modelled reach, was reworked to display local $|\vec{v}_{fish}|$. Correct behaviour of the code was tested in a small test scenario which was calculated by hand as well (Appendix A).

2.1.3. Indicators

Modelling fish pathways and velocities as described in section 2.1.1 & 2.1.2 yields spatially distributed results. Whereas allowing localisation of higher risk areas on small scales it complicates quantitative comparison of different scenarios and reaches. Hence, aggregation of the distributed results into single value indicators is introduced:

Path Length L_{75}
Introduced by Lüthy et al., unpub. the 75-percentile length of all total paths is calculated representing the distance a fish has to overcome while moving with its shifting habitat.

Habitat Shift HS_{75}
A fish following a path needs to travel the distance within the available time, which is defined by the ramping duration. The fish must be faster for a longer path or a shorter ramping duration. This speed is termed *Habitat Shift* (adapted from Lüthy et al., unpub.) and computed per path segment as defined in Equation 9. It corresponds to $|\vec{v}_{path}|$ in section 2.1.2. The smaller HS_{75}, the more time the fish have to find the new habitat. Hence, lower values are preferable.

$$HS = \frac{L_{Path,k}}{\Delta t_k} \tag{9}$$

Fraction of Disconnected Paths P_d
P_d is calculated by dividing the number of paths considered impassable, i.e. containing at least one cell where $|\vec{v}_{fish}| > v_{crit}$, by the total number of paths (Equation 10). Since all cells have the same area it is equivalent to the fraction of disconnected origin habitat, i.e. origin habitat from where a fish is unlikely to reach any target habitat.

$$P_d = \frac{n_{dp}}{n_p} \tag{10}$$

where
n_p number of paths [–] n_{dp} number of disconnected paths [–]

Weighted Habitat Loss WHL
A higher value for P_d does not necessarily imply higher stranding or drifting as it does not consider whether fish are present in the disconnected initial habitat. Without field mapping this information cannot be obtained but may be approximated: Assuming the suitability of a habitat to correspond to the likelihood of fish being present, more suitable areas becoming disconnected is more likely to cause stranding or drifting. Weighting the origin habitats being disconnected with their suitability extends P_d by this concept as shown in Equation 11. Habitat suitability CSI is computed by geometric mean considering preference curves of depth and velocity (Equation 12).

$$WHL = \frac{\sum_{i=1}^{n_{dp}} CSI_i * A_i}{\sum_{i=1}^{n_p} CSI_i * A_i} \quad (11) \qquad CSI_i = \sqrt{SI_{h,i} * SI_{v,i}} \quad (12)$$

where

CSI_i	composite suitability index of cell i $[-]$	A_i	Area of cell i $[m^2]$
$SI_{h,i}$	suitability index from depth $[-]$	$SI_{v,i}$	suitability index from velocity $[-]$

WHL is considered to quantify the risk of fish to either strand or drift while following their shifting habitat.

Weighted Connected Habitat WCH

The Habitat Suitability Index HSI, as defined in Equation 13, can be used to quantify the habitat availability within a river reach. Disconnected areas cannot provide persistent habitat under hydropeaking condition as fish will there either strand or drift away. Therefore, the concept is extended to only consider initial habitats which stay connected throughout the hydropeaking scenario. Equation 14 describes the resulting Weighted Connected Habitat WCH.

$$HSI = \frac{WUA}{A_{river}} = \frac{\sum_{i=1}^{n_p} CSI_i * A_i}{\sum_{i=1}^{n_p} A_i} \quad (13) \qquad WCH = \frac{(1 - WHL) * WUA}{A_{river}} \quad (14)$$

where

A_{river}	Wetted river area $[m^2]$	WUA	Weighted usable area $[m^2]$

WCH is considered to quantify the effectively available habitat under hydropeaking conditions.

The presented indicators need to feature the following properties:

- *Sensitivity*: Reacting to improving (or worsening) conditions by an increase (or decrease) in indicator value.
- *Relevance*: The captured change in river condition needs to be of relevance for the considered species
- *Consistency*: Comparable river conditions result in a similar indicator value regardless of circumstances (e.g. length of modelled reach).

During the sensitivity analysis (section 2.1.4) and the assessment of varying morphology (section 2.2.2) each indicator is tested for the three properties. Their calculation was implemented in the Java code. Correct behaviour of the code was tested in a small test scenario which was calculated by hand as well.

2.1.4. Sensitivity Analysis

The sensitivity analysis addresses two topics: Firstly, to understand the importance of the model parameters and their interactions. Secondly, to investigate indicator behaviour for changing conditions. The chosen approach follows Saltelli et al., 2008 implementing a variance based method computing Sobol indices. Parameter sets are created using Monte-Carlo sampling assuming uniform parameter distribution.

Analysed Parameters

Table 2 shows the six parameters investigated in the sensitivity analysis. For each parameter a possible value range was defined from which one value was randomly drawn per parameter set assuming an uniform distribution. The approach by Saltelli et al., 2008 requires the parameter sets to be sampled independently, hence possible value ranges for suitable and critical velocity as well as λ_{mid} and λ_{max} do not overlap. Otherwise constrains to prevent a suitable velocity larger the critical velocity or $\lambda_{\text{mid}} > \lambda_{\text{max}}$ would be required turning their sampling dependent.
The sensitivity analysis was applied to the *Kiesbankstrecke* at the Hasliaare (s. Section 2.2.1). A separate sensitivity analysis for up- and downramping was performed between 2 and 150 $\frac{\text{m}^3}{\text{s}}$ with a raster resolution of 0.25 m. Brown trout larvae was considered as species and their preference curves taken from Belaud et al., 1989 (fig. 7). v_{mid} and λ_{min} were fixed to 0.4 $\frac{\text{m}}{\text{s}}$ and 0.0 respectively.

Sobol Indices

Sensitivity indices are computed with a variance based method as described by Saltelli et al., 2008. Two matrices A and B are defined each containing N randomly sampled parameter sets (Equation 15). Each row contains one parameter set whereas each column corresponds to one of the k considered parameters. For each parameter i a new matrix C_i is generated as shown in Equation 16. It is equivalent to matrix B except for the i-th column which is taken from of matrix A.

Parameter	Minimum	Maximum	Source
Δt $\left[\frac{\text{h*s}}{\text{m}^3}\right]$	0.006	0.356	Juárez et al., 2019; Larrieu and Pasternack, 2021
v_{suit} $\left[\frac{\text{m}}{\text{s}}\right]$	0.020	0.270	Belaud et al., 1989
v_{crit} $\left[\frac{\text{m}}{\text{s}}\right]$	0.300	0.600	Heggenes, 1988
h_{min} [m]	0.001	0.021	Belaud et al., 1989; Lüthy et al., unpub.
λ_{mid} [−]	0.000	1.000	Lüthy et al., unpub.
λ_{max} [−]	1.000	3.500	Lüthy et al., unpub.

Table 2: Investigated parameters in the sensitivity analysis. Parameter sets are sampled assuming a uniform distribution between minimum and maximum value. Sources used to define the value range are also provided.

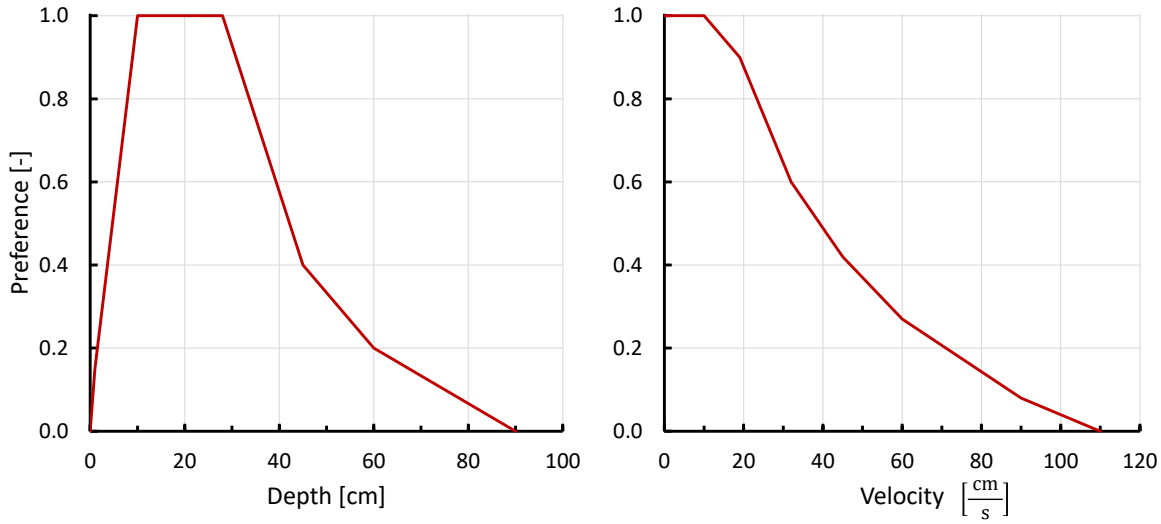

(a) Depth

(b) Velocity

Figure 7: Preference curves according to Belaud et al., 1989 for brown trout larvae.

$$A = \begin{bmatrix} x_1^{(1)} & x_2^{(1)} & \cdots & x_k^{(1)} \\ x_1^{(2)} & x_2^{(2)} & \cdots & x_k^{(2)} \\ \vdots & \vdots & & \vdots \\ x_1^{(N-1)} & x_2^{(N-1)} & \cdots & x_k^{(N-1)} \\ x_1^{(N)} & x_2^{(N)} & \cdots & x_k^{(N)} \end{bmatrix} \qquad B = \begin{bmatrix} x_{k+1}^{(1)} & x_{k+2}^{(1)} & \cdots & x_{2k}^{(1)} \\ x_{k+1}^{(2)} & x_{k+2}^{(2)} & \cdots & x_{2k}^{(2)} \\ \vdots & \vdots & & \vdots \\ x_{k+1}^{(N-1)} & x_{k+2}^{(N-1)} & \cdots & x_{2k}^{(N-1)} \\ x_{k+1}^{(N)} & x_{k+2}^{(N)} & \cdots & x_{2k}^{(N)} \end{bmatrix} \tag{15}$$

$$C_i = \begin{bmatrix} x_{k+1}^{(1)} & x_{k+2}^{(1)} & \cdots & x_i^{(1)} & \cdots & x_{2k}^{(1)} \\ x_{k+1}^{(2)} & x_{k+2}^{(2)} & \cdots & x_i^{(2)} & \cdots & x_{2k}^{(2)} \\ \vdots & \vdots & & \vdots & & \vdots \\ x_{k+1}^{(N-1)} & x_{k+2}^{(N-1)} & \cdots & x_i^{(N-1)} & \cdots & x_{2k}^{(N-1)} \\ x_{k+1}^{(N)} & x_{k+2}^{(N)} & \cdots & x_i^{(N)} & \cdots & x_{2k}^{(N)} \end{bmatrix} \tag{16}$$

where

x_i	value of parameter i
k	number of parameters
N	sample size

The model is run with all parameter sets defined by the matrices resulting in $N * (k+2)$ runs. Calculated model indicator values are stored in result vectors $\vec{y}_{A,j}$, $\vec{y}_{B,j}$ and $\vec{y}_{C_i,j}$, where j denotes the considered indicator. Computing the variance of each result vector and quantifying the differences between them, i.e. differences from changing all values except for parameter i ($y_{C_i,j} \leftrightarrow y_{A,j}$) and changing only values of parameter i respectively ($y_{C_i,j} \leftrightarrow y_{B,j}$), allows estimation of the Sobol sensitivity indices.

The first-order index $S_{i,j}$ quantifies the contribution of parameter i to the model variance of indicator j (Equation 17). It provides by how much the variance could be reduced by

setting parameter i to a fixed value, hence is also called main effect. A difference in value of parameter i may influence the sensitivity of any other parameter. The total-effect index $S_{T_i,j}$ includes these indirect contribution to the model variance (Equation 18).

$$S_{i,j} = \frac{\vec{y}_{A,j} \cdot \vec{y}_{C_i,j} - f_{0,j}^2}{\vec{y}_{A,j} \cdot \vec{y}_{A,j} - f_{0,j}^2} \qquad (17) \qquad S_{T_i,j} = 1 - \frac{\vec{y}_{B,j} \cdot \vec{y}_{C_i,j} - f_{0,j}^2}{\vec{y}_{A,j} \cdot \vec{y}_{A,j} - f_{0,j}^2} \qquad (18)$$

where

$$f_{0,j}^2 = \left(\frac{1}{N} \sum_{n=1}^{N} y_{A,j}^{(n)} \right)^2$$

$S_{i,j}$	first-order index of parameter i for indicator j
$S_{T_i,j}$	total-effect index of parameter i for indicator j
$\vec{y}_{A,j}$	result vector of matrix A for indicator j
$\vec{y}_{B,j}$	result vector of matrix B for indicator j
$\vec{y}_{C_i,j}$	result vector of matrix C_i for indicator j
$f_{0,j}^2$	squared mean of $\vec{y}_{A,j}$

By their definition three conditions arise for $S_{i,j}$ and $S_{T_i,j}$ which are given in Equation 19, 20 & 21 and used to verify the plausibility of the sensitivity analysis results.

$$\sum_{i=1}^{k} S_{i,j} \leq 1 \qquad (19) \qquad \sum_{i=1}^{k} S_{T_i,j} \geq 1 \qquad (20) \qquad S_{T_i,j} \geq S_{i,j} \mid \forall i \in k \qquad (21)$$

2.1.5. Validation

The performance of the model was not investigated previously. As a first estimate the model was applied to a river reach for which hydraulic data and locations of observed fish stranding are available. Juárez et al., 2019 modelled a two kilometre long reach of the Storåne River, Norway, and provide the location of observed fish stranding events. Section 2.2.1 describes the Storåne River reach in more detail.

Parameter	Unit	Value
Duration	$\frac{h*s}{m^3}$	0.002
Suitable velocity	$\frac{m}{s}$	0.300
Middle velocity	$\frac{m}{s}$	0.400
Critical velocity	$\frac{m}{s}$	0.500
minimum depth	m	0.010
λ_{min}	-	0.000
λ_{mid}	-	0.600
λ_{max}	-	2.000

Table 3: Parameters for model validation and application.

Brown trout was chosen to be modelled as itis the species of concern at the Storåne River (Juárez et al., 2019). Due to their larger vulnerability swimming capacities and preference curves of larvae were selected. The most severe realistic downramping scenario, as described by Juárez et al., 2019, consists of a parallel, rapid shutdown from three operating turbines to residual flow. Consequently, the discharge decreases from 51 $\frac{m^3}{s}$ (three turbines) to 6 $\frac{m^3}{s}$ (residual flow) in 5 minutes (0.002 $\frac{h*s}{m^3}$), with hydraulic data being available for 51 $\frac{m^3}{s}$, 36 $\frac{m^3}{s}$, 21 $\frac{m^3}{s}$ and 6 $\frac{m^3}{s}$. The combination of the life stage most prone to stranding with the most severe realistic downramping scenario is considered to compensate for optimum paths being calculated whereas non-optimal fish behaviour is expected in reality. Table 3 summarises the model settings and Figure 7 shows the selected preference curves.

Locations with stranding events recorded by Juárez et al., 2019 were identified in the model result image. The performance of the model was rated positively if stranding risk was indicated at these sites, e.g. by disconnected origin habitat, and negatively otherwise.

2.2. Model Application

After the validation of the FiER model it was used to investigate the impact of different morphologies on fish stranding and drifting risk (section 2.2.2). Additionally, areas with higher risk were identified in the Storåne River applying two different approaches as explained in section 2.2.3. An overview of the selected study sites is given in section 2.2.1.

2.2.1. Study Sites

The study sites were selected to span river morphologies with varying degrees of human alteration while being exposed to hydropeaking. The lower part of the Hasliaare River, the section of the Swiss river Aare in the Hasli Valley, was straightened between Meiringen and Lake Brienz between 1866 and 1883 (Roth, 2019). As a result the entire reach has a strongly altered morphology (Schweizer et al., 2013). Since the construction of a hydropower plant at Innertkirchen in 1942 it is also subject to hydropeaking (KWO, 2022). Based on their morphology four different reaches can be identified of which three, channel, groyne and gravel bars, are investigated in this study (s. Figure 8).

In contrast to the strongly altered Hasliaare River the 2 kilometre long natural braided reach of the Storåne River, Norway, upstream of Lake Hovsfjorden enables comparison to a natural morphology (Juárez et al., 2019). With the Hol 1 Power Station outlet being located 400m upstream of the Storåne River reach it is also exposed to hydropeaking, as shown in Figure 13.

The Hasliaare System

The Hasliaare forms the uppermost part of the Aare River in Switzerland. It is located in the southeastern part of the Canton Bern reaching from the river's source at the glaciers Unteraar and Oberaar to its esturay into Lake Brienz. Its catchment covers a steep alpine area of 556km^2 ranging from 550 m a.s.l. to 4130 m a.s.l. with an average altitude of 2126 m a.s.l. (FOEN, 2022). Land cover mainly consists of rocks (28%), glaciers (20%), grassy & herbaceous vegetation (20%) and forests (15%) with an average slope of 28°. Consequently, the hydrologic regime features low flows during winter (14 $\frac{m^3}{s}$[1]) and high flows in summer (68 $\frac{m^3}{s}$[2]).

The hydropower company Kraftwerke Oberhasli AG (KWO) operates a complex system of dams, intakes, tunnels and hydropower stations producing 2'400 GWh of electricity

[1] 1905 - 2017 average in DJF (FOEN, 2022)
[2] 1905 - 2017 average in JJA (FOEN, 2022)

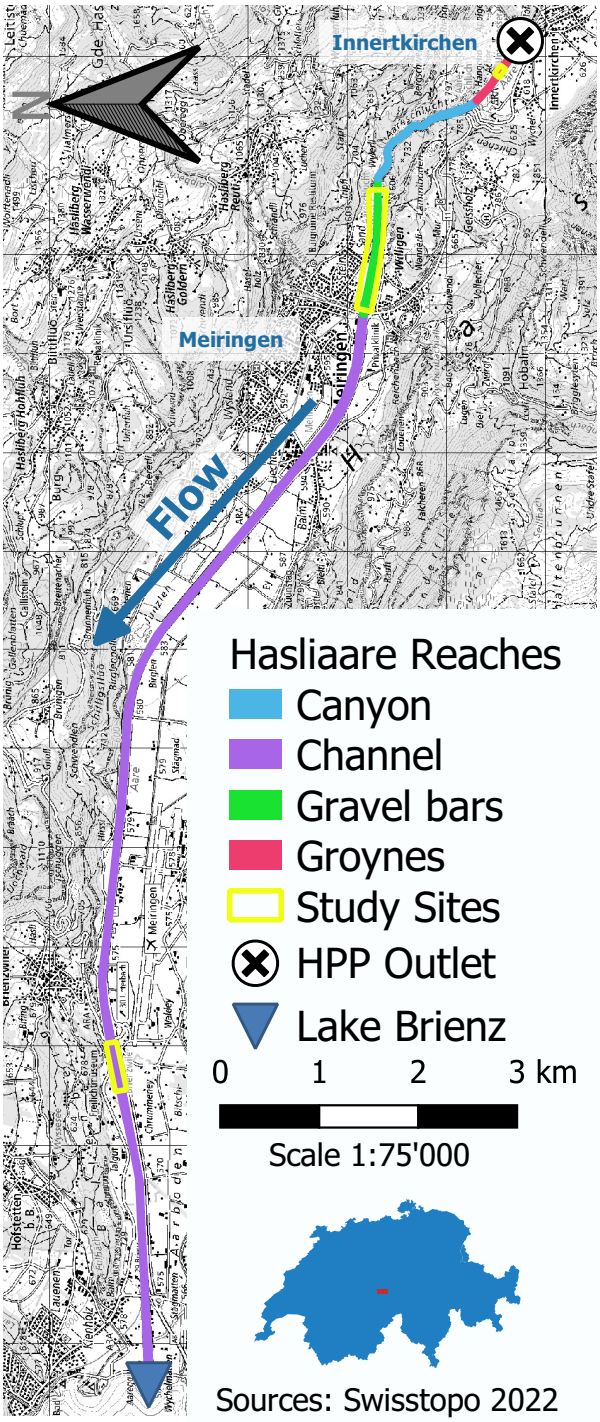

Figure 8: Location of reaches and study sites along the Hasliaare River.

Figure 9: Channelised reach at the Hasliaare River.

Figure 10: Groyne reach at the Hasliaare River.

Figure 11: Gravel bar reach at the Hasliaare River.

Figure 12: Naturally braided reach at the Storåne River.

per year in the catchment (KWO, 2022). The hydropower plants Innertkirchen 1 and 1E, with a maximum capacity of 43 $\frac{m^3}{s}$ and 26 $\frac{m^3}{s}$ respectively, drain into the Hasliaare River at Innertkirchen causing hydropeaking impacting the hydrologic regime on a sub-daily scale.

Hasliaare River - Channelised Reach

The channelised part of the Hasliaare River reaches 11.8 km from Meiringen to the estuary at Lake Brienz (Bieri, 2012). It has a trapezoidal cross-section with steep banks and a fast, monotonous flow (Figure 9). A 500 m long and 36 m wide section of the reach is investigated in this study as shown in Figure 8.

Hasliaare River - Groyne Reach

Between the KWO hydropower station outlet and the Aareschlucht canyon groynes are present on either side of the river (Bieri, 2012). In the main channel high flow velocities are present whereas slower flows are observed between the groynes (Figure 10). The section investigated in the model spans a length of 105 m with a width of 45 m. Figure 8 provides its exact location.

Hasliaare River - Gravel Bars Reach

Downstream of the Aareschlucht canyon the river is wider until Meiringen allowing alternate bars to form (Figure 11). Consequently, flow fields are more varied than in the channelised and groyne reach. Six gravel bars are present within the 1230 m long and 85 m wide section investigated in this study (s. Figure 8).

For all three reaches raster data for water depth and velocity was provided by KWO spanning a discharge range from 1.5 $\frac{m^3}{s}$ to 150 $\frac{m^3}{s}$. Data for 22 intermediate discharges was also provided resulting in a total of 24 data sets. They were obtained from hydraulic modelling and have a spatial resolution of 0.25 m.

The Hol 1 Storåne System

At Lake Hovsfjorden the Storåne River drains a catchment of roughly 725 km^2 of which 91% lays above 900 m a.s.l. (ECOHZ, 2022). The 2.4 km section of the Storåne River upstream of the lake is affected by hydropeaking from the Hol 1 power station, Buskerud county, Norway. It consists of four Francis turbines with capacity of 15 $\frac{m^3}{s}$ each and a total annual production of 850 GWh per year (Hafslund, 2022). It is connected to two reservoirs with a drop of 380 m and 407 m and a combined storage volume of 850 million m^3 (Hafslund, 2022; Juárez et al., 2019). It has been in operation since 1956. Observed rapid discharge fluctuations downstream of the outlet vary between 281 and 331 occurrences per year[3].

[3] 2012 - 2017

Storåne River - Natural Braided Reach

The first 400 m downstream of the Hol 1 power station consist of a trapezoidal channel (Juárez et al., 2019). In the remaining 2 km to Lake Hovsfjorden three main islands, Ellingøyne, Gjerdeøyne and Mørkaøyne, together with multiple side channels, form a natural braided morphology as shown in Figure 12 & 13. River width varies between 10 m and 150 m. The entire reach is accessible for brown trouts (*Salmon Trutta*) migration upstream from Lake Hovsfjorden.

Juárez et al., 2019 provided the results of their hydraulic simulation of the Storåne River reach. From this data the required raster data sets were derived in QGIS (QGIS, 2022) at a spatial resolution of 1 m. The data includes water depth and flow velocities for 51 $\frac{m^3}{s}$, 36 $\frac{m^3}{s}$, 21 $\frac{m^3}{s}$ and 6 $\frac{m^3}{s}$ corresponding to 3, 2, 1 and 0 operating turbines (Juárez et al., 2019).

2.2.2. Influence of Morphology on Stranding and Drifting Risk

The model was used to investigate differences in fish stranding and drifting risk due to variation in bed topography, represented by river morphology. Comparable hydraulic scenarios were applied to all four sites described in section 2.2.1 modelling both up- and downramping. To characterise the hydraulics spatially for each reach the median μ_{50}, the standard deviation σ and the coefficient of varation $CV = \frac{\sigma}{\mu}$ of depth and velocity were computed. Brown trout larvae was chosen as fish species as it is of relevance at all sites (Lüthy et al., unpub. Juárez et al., 2019).

The most severe realistic scenario described by Juárez et al., 2019, i.e. a discharge change of 45 $\frac{m^3}{s}$ in 5 minutes (compare section 2.1.5), was selected for all four sites. Accordingly, the discharge ranged from 5 $\frac{m^3}{s}$ to 50 $\frac{m^3}{s}$ and from 6 $\frac{m^3}{s}$ to 51 $\frac{m^3}{s}$ for the Hasliaare sites and the Storåne River site respectively. At all four sites this roughly corresponds to a range between the mean annual minimum and the 90th-percentile of the discharge (Juárez et al., 2019[4], Lüthy et al., unpub.[5]), hence the ramping scenarios are considered comparable.

The model was applied to all sites considering all available discharges within the specified range (s. section 2.2.1). Parameter values are provided in Table 3 and preference curves in Figure 7 (Belaud et al., 1989). With the same parameter values and comparable hydraulic conditions at all sites the obtained indicator values were compared to assess the influence of the morphology on the stranding and drifting risk.

2.2.3. Identifying Higher Risk Areas in the Storåne River

Stranding and drifting risk vary throughout a river reach. Using the model areas with higher risk can be identified allowing river managers to focus their attention where it

[4] 2010 - 2017
[5] 2015 - 2019

is most needed. This study shows two different approaches to identify higher risk areas in the Storåne River using the FiER model. Section 2.2.1 provides more details on the Storåne River reach.

River Segmentation Analysis

River reaches may be split into segments depending on a decisive criterion. Here, the Storåne River reach was divided into segments with one or multiple channels, as higher risk is expected with the more complex morphology of multiple channels. In total the reach was split into eight segments with four segments per channel type (s. Figure 13).

To characterise the segments the median μ_{50}, the standard deviation σ and the coefficient of variation $CV = \frac{\sigma}{\mu}$ of depth and velocity were computed for each. The model was run separately per segment as well as for the entire reach. The same parameter settings, hydraulic scenario and preference curves as for the validation were used (s. Table 3 & Figure 7) and applied to both up- and downramping. Resulting indicator values were compared to identify segments with higher risk and to investigate the effect of channel type on fish stranding and drifting risk.

Stranding Patch Analysis

Whereas the *River Segmentation Analysis* allows for an easily understandable division of the river reach the FiER model enables spatial analysis on smaller scales. Patches with known risk for stranding, e.g. from observed stranding events, can be identified in the result image. Throughout the reach patches of similar characteristics can be located as higher risk areas.
Using stranding events documented by Juárez et al., 2019 and the model result image as obtained during validation (s. Section 2.1.5) this approach was applied to the Storåne River reach. In a first step the location of the stranding events was identified in the result image and the surrounding area manually characterised into different patch types. Secondly, the entire river reach was manually searched for patches with similar characteristics and labelled with the respective patch type. Finally, their location was compared with the results of the *River Segmentation Analysis* by counting the number of identified patches per segment.

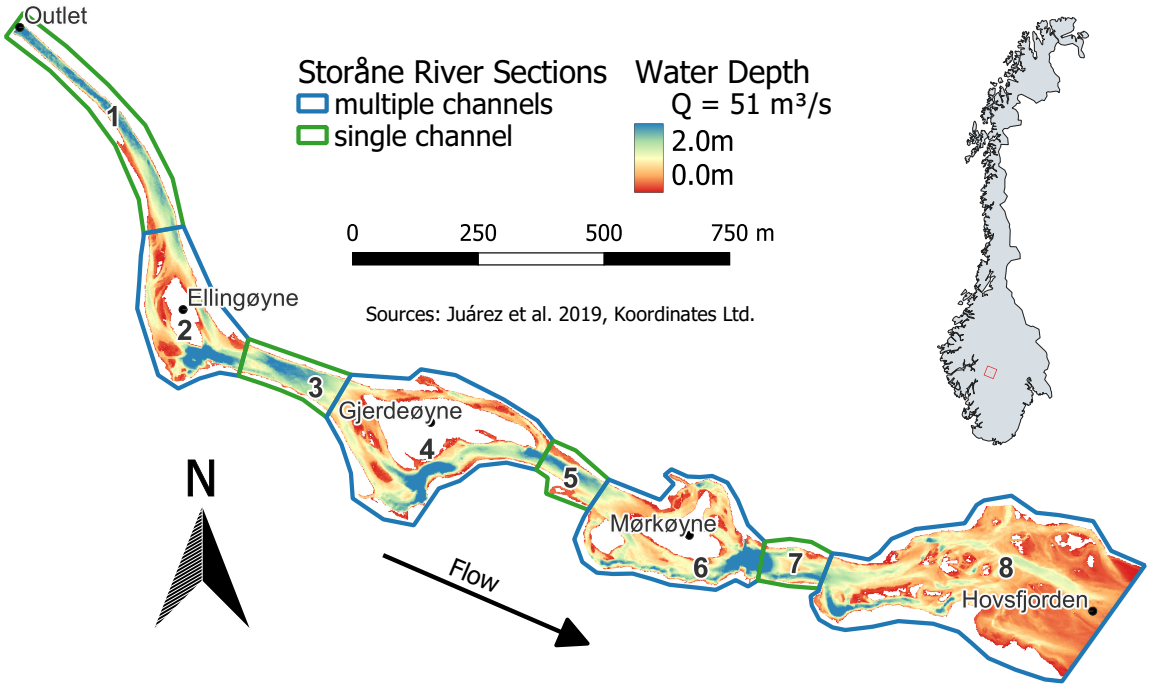

Figure 13: Location of the Storåne River reach. The power station outlet, the three main islands and the estuary into Lake Hovsfjorden are labelled. The numbers indicate the defined sections.

3. Results

The outcome of analysing the FiER model is presented in Section 3.1 before showing the results obtained by applying the model on the studied reaches (Section 3.2).

3.1. Fish Escaping Routes Model

Correct implementation of the model in Java was tested successfully for both test cases, i.e. fish velocity and indicator computation. More details are provided in Appendix A. Section 3.1.1 presents the results of the sensitivity analysis and Section 3.1.2 provides the validation outcome.

3.1.1. Sensitivity Analysis

For the upramping sensitivity analysis a sample size of $N = 2'050$ resulted in 16'400 model runs. Figure 14 shows the derived Sobol sensitivity indices for all parameters and indicators. With the sole exception of indicator WCH the plausibility conditions 19, 20 & 21 are satisfied. For the downramping scenario with a sample size of $N = 2'000$ these conditions were violated in most cases as can be seen in Figure 20, Appendix B. Therefore, the results for the downramping scenario are considered unreliable and were excluded from further analysis.

The two indicators P_d and WHL show almost identical results for both sensitivity indices. By far the strongest influence on the two indicators has v_{crit} with $S_{v_{crit}} = 0.8$ (Figure 14a). A much lower effect comes from Δt ($S_{\Delta t} = 0.1$). The remaining four parameters, v_{suit}, λ_{mid}, λ_{max} and h_{min} are negligible with $S_i \approx 0.0$. Their unexpected slightly negative values are attributed to the randomness associated with the Monte-Carlo approach and considered to be within the uncertainty of this analysis. Results for WCH have to be interpreted with care, as they do not fulfil the plausibility conditions. Generally, they appear to be shifted upwards compared to P_d and WHL but indicating a similar ranking of the parameter sensitivities. In contrast to WCH the first-order sensitivities for L_{75} seem shifted downwards with unexpected negative values. Similarly, these results are considered less reliable: The strongest impact on L_{75} has λ_{max} with $S_{\lambda_{max}} = 0.6$, followed by v_{crit}, $S_{v_{crit}} = 0.1$, and λ_{mid} with $S_{\lambda_{mid}} = 0.0$. Assuming a downward shift Δt, v_{suit} and h_{min} are considered negligible. Finally, only Δt seems to be of importance for HSI_{75} with $S_{\Delta t} = 0.9$.

3.1.2. Validation

The location of the four stranding events observed by Juárez et al., 2019 are marked in the result image in Figure 15 which was obtained by modelling the most severe realistic downramping scenario as described in Section 2.1.5. Box 3 gives assistance to interpret result images created by the model.

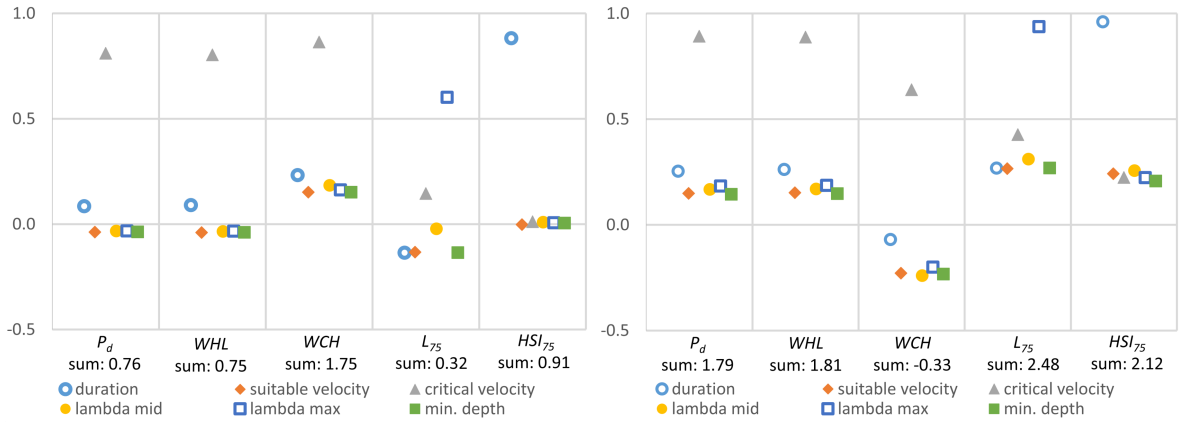

(a) First-order index S_i (b) Total-effect index S_{T_i}

Figure 14: Sobol sensitivity indices for the upramping scenario at the Hasliaare channel reach. For indicator *WCH* they do not fulfil condition 19, 20 & 21.

Box 3: Reading Result Images

The model creates one image per run illustrating the spatial distribution of the results. One example showing a upramping scenario is provided in the image below. White areas are always, grey and black areas never inundated. In between a gradient from bright to dark brown indicates the progression of the waterline. The target habitats, i.e. the suitable areas of the last input raster set, are shown in blue. In the example these are located along the river banks. Origin habitats and paths share the same colour code but are distinguished by their opacity.

Origin habitats have more saturated colours than paths. This can bee seen in the image at the marked origin habitat in the middle of river from which a path leads to the upper left. The colours indicate the fish velocity at this point where green corresponds to suitable, yellow to subcritical and red to supercritical. Hence, fish in the marked origin habitat start their path swimming suitable and subcritical velocities respectively. However, since the path includes supercritical velocities the origin habitat is disconnected. Additionally, origin habitats where no path was found are coloured in pink as can be seen in Figure 15.

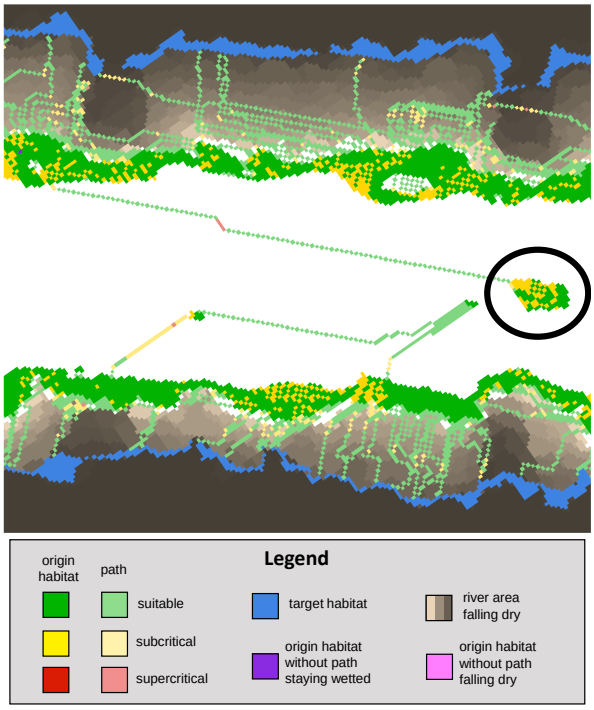

Two stranding events, *E1* and *E2*, happened directly up- and downstream of Ellingøyne Island (Figure 15II). At *E1* the FiER model shows a side channel falling dry in a complex pattern with a large, adjacent origin habitat. For most of the origin habitat no path was found. Downstream of Ellingøyne Island, at location *E2*, observed fish stranding coincides with a larger origin habitat falling dry with no path found. A similar pattern is observed at Gjerdeøyne Island in Figure 15III (location *G*). No clear pattern can be determined downstream of Mørkaøyne Island at point *M* (Figure 15IV). Besides the locations *E1*, *E2*, *M* and *G* several similar patches are found without recorded stranding events (s. Section 3.2.2).

3.2. Model Application

Investigating different morphologies under up- and downramping conditions yielded results as provided in Section 3.2.1. Areas of higher risk are presented in Section 3.2.2.

3.2.1. Influence of Morphology on Stranding and Drifting Risk

The result images for all studied reaches and scenarios are provided in Appendix C. Differences in morphologies between the reaches are also present in their hydraulic parameters (Table 4). For low discharges, median water depth decreases with increasingly complex morphology, i.e. from the channelised to the naturally braided reach. Median velocity is the same for the channelised and the groynes reach, but decreases for the gravel bars and the naturally braided reach. Variation of water depth and velocity increase with morphological complexity. At higher discharges median water depth is higher and still decreases with increasingly complex morphology, however, its variation is similar for all but the naturally braided reach. Median velocity shows a similar behaviour whereas its variation increases from gravels bars, over the channelised and groynes to the naturally braided reach.

The four studied channels differ in size as can be seen in Table 5 from the wetted area. Correspondingly, WUA at low discharge is largest for the naturally braided reach, followed by the gravel bars, channelised and groynes reach. Being independent from the area HSI increases with reach complexity, as do P_d, WHL and L_{75} during upramping (Table 5). The lowest WCH is observed for the channelised reach, followed by gravel bars, groynes and the naturally braided reach, similarly for HS_{75}. A different pattern is observed for downramping where the gravel bars reach shows the lowest values for HSI, P_d and WHL followed by the groynes, channelised and naturally braided reach (Table 6). For the other indicators the order of reaches varies with the groynes and naturally braided reach tending to show higher, the channelised and gravel bars reach lower values. All reaches except the channelised reach have a higher HSI for lower discharge. P_d, WHL and WCH show more desirable values during the upramping scenario for all reaches although L_{75} and HS_{75} are higher.

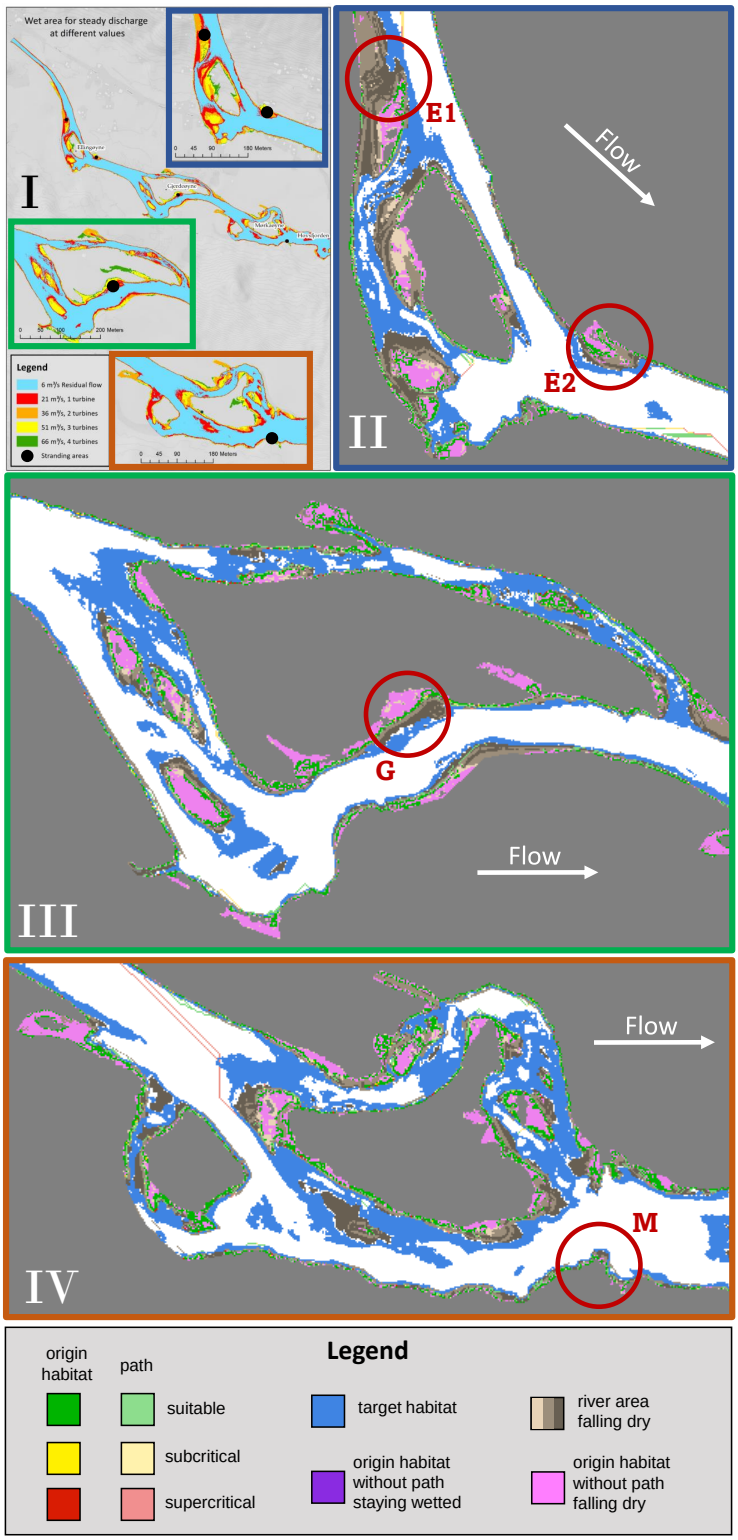

Figure 15: Stranding events observed by Juárez et al., 2019 (I) are marked in the result image: E1 & E2 (II), G (III) and M (IV).

3.2.2. Identifying Higher Risk Areas in the Storåne River

As mentioned in Section 3.1.2 similar patterns as observed at the sites of stranding events are found throughout the result image of the downramping scenario of the Storåne River reach.

River Segmentation Analysis

Single channel sections (SCS) show deeper water depth ($\bar{\mu}_{50,h,s} = 1.28m$) than sections with multiple channels (MCS, $\bar{\mu}_{50,h,m} = 0.75m$), whereas depth variation is higher for MCS (Table 7). Similarly, flow velocity is higher for SCS ($\bar{\mu}_{50,v,s} = 0.80m$) compared to MCS ($\bar{\mu}_{50,h,s} = 0.58m$). Variation in velocity is also higher for MCS. Additionally, HSI for MCS is roughly double the HSI value for SCS at both high and low flows (Table 8).

In the downramping scenario SCS show smaller disconnection of habitats (P_d, WHL) and lower WCH. Whereas the paths, i.e. L_{75}, are longer for SCS HS_{75} is almost identical for both channel types. During upramping more disconnection occurs for SCS (P_d, WHL) but WCH is still higher for MCS. The difference in path length L_{75} is less pronounced than during downramping and HS_{75} is now slightly higher for MCS. Generally, indicator values for SCS and MCS are in a similar range. Hydraulic characteristics and model indicator for all sections are provided in Table 9, Appendix D.

Section	Unit	single	multiple	all
$\mu_{50,h}$ Q^*_{high}	m	1.28	0.75	0.75
CV_h Q^*_{high}	–	48.4%	99.3%	96.0%
$\mu_{50,v}$ Q^*_{high}	$\frac{m}{s}$	0.80	0.58	0.54
CV_v Q^*_{high}	–	40.3%	61.5%	70.4%
No. risk areas		0.50	4.75	21

* Q_{high} describes 51 $\frac{m^3}{s}$

Table 7: Hydraulic characteristics for the single and multiple channel sections (mean) and modelling the entire reach.

Stranding Patch Analysis

Two types of patches were identified at the sites of stranding as presented in Figure 16. At site *E1* a complex pattern in a dewatering side channel is observed adjacent to an origin habitat for which predominantly no path was found. The second type was observed at sites *E2* and *G* as a larger patch of origin habitat becomes disconnected while clearly separated from the remaining channel. This type is found 19 times throughout the reach with the majority being located in the estuary section 8 (Figure 17). The complex dewatering type was found two times. Of 21 risk areas 19 were found in a multiple channel section as summarised in Table 7.

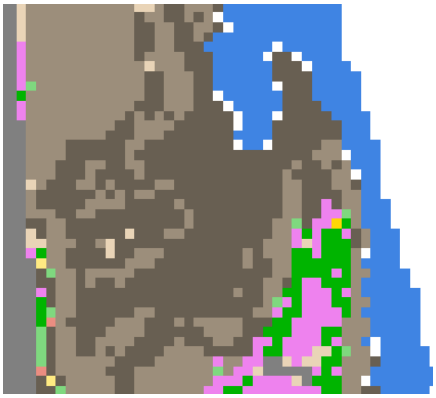

(a) Complex dewatering

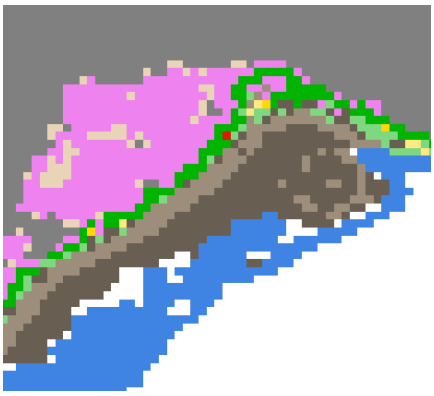

(b) Disconnected habitat

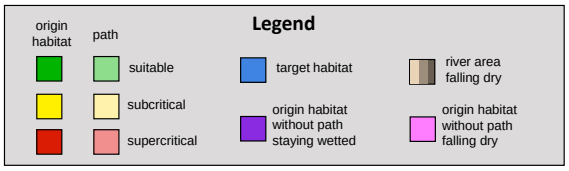

Figure 16: Two patch types were identified at the sites of observed stranding: Complex dewatering with adjacent origin habitat (a) and a large patch of disconnected origin habitat (b).

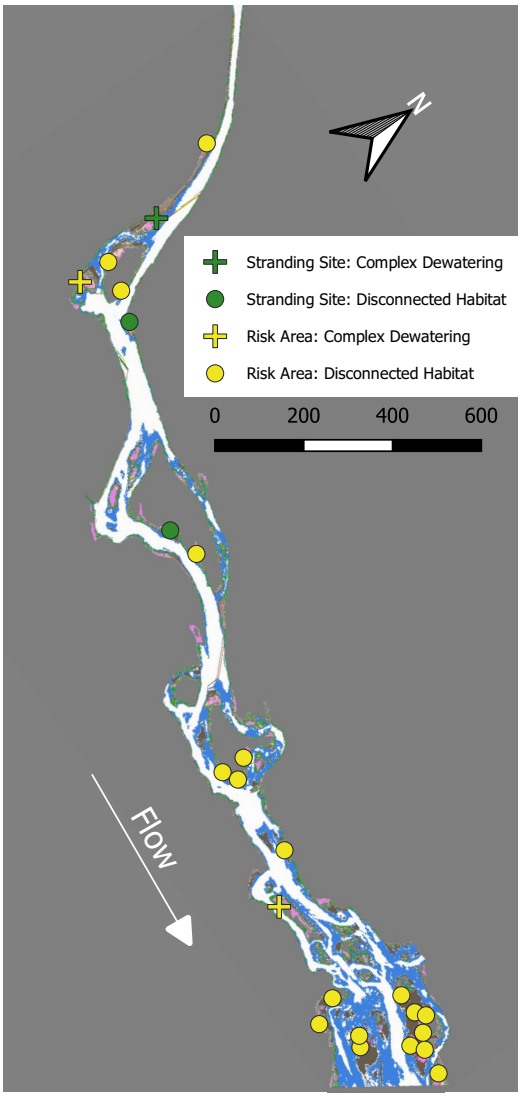

Figure 17: Location of observed stranding sites (green) and identified risk areas (yellow) per patch type. Most risk areas appear in the estuary region.

Indicator	Unit	Reach			
		Channelised	Groynes	Gravel Bars	Naturally Braided
μ_{50} depth Q^*_{low}	m	0.50	0.37	0.22	0.32
σ depth Q^*_{low}	m	0.14	0.14	0.15	0.64
CV depth Q^*_{low}	–	28.0%	37.8%	68.2%	200.0%
μ_{50} velocity Q^*_{low}	$\frac{m}{s}$	0.75	0.75	0.63	0.15
σ velocity Q^*_{low}	$\frac{m}{s}$	0.24	0.33	0.32	0.20
CV velocity Q^*_{low}	–	32.0%	44.0%	50.8%	133.3%
μ_{50} depth Q^{**}_{high}	m	1.81	1.24	0.84	0.75
σ depth Q^{**}_{high}	m	0.67	0.45	0.29	0.72
CV depth Q^{**}_{high}	–	37.0%	36.3%	34.5%	96.0%
μ_{50} velocity Q^{**}_{high}	$\frac{m}{s}$	1.83	1.71	1.73	0.54
σ velocity Q^{**}_{high}	$\frac{m}{s}$	0.76	0.94	0.59	0.38
CV velocity Q^{**}_{high}	–	41.5%	55.0%	34.1%	70.4%

* Q_{low} describes 6 $\frac{m^3}{s}$ for naturally braided reach, 5 $\frac{m^3}{s}$ for all other reaches

** Q_{high} describes 51 $\frac{m^3}{s}$ for naturally braided reach, 50 $\frac{m^3}{s}$ for all other reaches

Table 4: Median μ_{50}, standard deviation σ and coefficient of variation CV for flow depth and velocity describe the hydraulics of the studied reaches for the highest (Q_{high}) and lowest discharge (Q_{low}) investigated

Indicator	Unit	Reach			
		Channelised	Groynes	Gravel Bars	Naturally Braided
Wetted area Q^*_{low}	m^2	7'921	2'235	38'619	219'150
WUA Q^*_{low}	m^2	441	230	4'037	62'557
HSI Q^*_{low}	–	5.6%	10.3%	10.5%	28.6%
P_d	–	0.0%	0.9%	21.6%	26.7%
WHL	–	0.0%	2.1%	19.8%	25.9%
WCH	–	5.6%	10.2%	8.4%	21.2%
L_{75}	m	5.0	6.5	18.6	43.7
HS_{75}	$\frac{m}{h}$	76.2	65.6	76.9	333.0

* Q_{low} describes 6 $\frac{m^3}{s}$ for naturally braided reach, 5 $\frac{m^3}{s}$ for all other reaches

Table 5: Calculated indicators for the upramping scenario of the studied reaches. Wetted area, Weighted Usable Area WUA and Habitat Suitability Index HSI are calculated for the first discharge of the scenario.

Indicator	Unit	Reach			
		Channelised	Groynes	Gravel Bars	Naturally Braided
Wetted area Q^*_{high}	m^2	10'042	2'902	44'246	240'153
WUA Q^*_{high}	m^2	868	217	1'859	27'183
HSI Q^*_{high}	–	8.6%	7.5%	4.2%	11.3%
P_d	–	52.4%	35.0%	26.2%	57.0%
WHL	–	53.8%	35.4%	26.5%	56.2%
WCH	–	4.0%	4.8%	3.1%	5.0%
L_{75}	m	0.85	1.21	1.06	3.51
HS_{75}	$\frac{m}{h}$	27.1	38.0	0.00	36.0

* Q_{high} describes 51 $\frac{m^3}{s}$ for naturally braided reach, 50 $\frac{m^3}{s}$ for all other reaches

Table 6: Calculated indicators for the downramping scenario of the studied reaches. Wetted area, Weighted Usable Area WUA and Habitat Suitability Index HSI are calculated for the first discharge of the scenario.

	Unit	upramping*			downramping**		
		single	multiple	all	single	multiple	all
Wetted Area	m^2	9'592	45'194	219'150	10'554	49'485	240'153
WUA	m^2	1'239	14'400	62'557	654	6'142	27'183
HSI	–	14.0%	28.6%	28.6%	6.9%	12.6%	11.3%
P_d	–	34.9%	27.9%	26.7%	45.5%	57.0%	57.0%
WHL	–	34.8%	27.0%	25.9%	45.7%	56.0%	56.2%
WCH	–	9.2%	21.1%	21.2%	3.0%	5.5%	5.0%
$L75$	m	50.31	45.67	43.7	5.12	3.59	3.51
HS_{75}	m	362.16	398.49	333.01	27.07	27.06	35.98

* Wetted Area, WUA and HSI for 6$\frac{\mathrm{m}^3}{\mathrm{s}}$ ** Wetted Area, WUA and HSI for 51$\frac{\mathrm{m}^3}{\mathrm{s}}$

Table 8: Indicators for the single and multiple channel sections (mean) and modelling the entire reach during up- and downramping.

4. Discussion

In Section 4.1 the model is discussed before moving to its applications in Section 4.2.

4.1. Fish Escaping Routes Model

Sensitivity analysis and validation are discussed in Section 4.1.1 and 4.1.2 respectively. Limitations of the model are presented in Section 4.1.3.

4.1.1. Sensitivity Analysis

Almost identical sensitivity results for P_d and WHL are due to their similar definitions. As all cells are of the same size P_d corresponds to a WHL with constant CSI. Differences in their indicator values come solely from varying CSI (s. Eq. 11 & 12) which is independent from the parameters considered in the sensitivity analysis. Their high sensitivity to v_{crit} could stem from its influence on both the cost calculation during path-finding (s. Section 2.1.1) and on the distinction into connected or disconnected habitat (s. Section 2.1.2). v_{suit} influences the cost calculation in a similar way, i.e. the dynamics of the exponential probability function, but is not decisive when distinguishing habitat connectivity. Hence, its negligible sensitivity suggests that the high sensitivity of v_{crit} arises from its impact on the distinction. This implies a low sensitivity of the path-finding algorithm to v_{crit} and v_{suit}, which is supported by the low sensitivity of L_{75} and HS_{75} to theses parameters. Furthermore, their by far lower sensitivity to Δ_t indicates that P_d and WHL are governed by the flow field rather than ramping speed. Sensitivities obtained for WCH show the same behaviour, which was expected due to the similar structure of the indicators, further supporting the statements despite the reduced reliability of the obtained WCH sensitivities.

The indicator L_{75} only considers the obtained paths, hence is not affected by the parameters impact on $|\vec{v}_{fish}|$. Therefore, assuming a shift in its sensitivities appears reasonable as Δ_t, which is not used in the calculation of the paths, should have per definition a value of $S_{\Delta_t} = 0$. L_{75} is sensitive to the parameters governing the dynamic exponential function, which is reasonable as it directly influences cost calculation, hence the paths. Although also defining the dynamics of the exponential function v_{suit} has a negligible influence on L_{75}. This observation may be different if either a larger range for v_{suit} would be sampled or other reaches would be modelled since most flow velocities at higher discharges exceeded its sample range (Table 2 & 4). HS_{75} high sensitivity to Δ_t is due to its linear relation as seen in Equation 9 potentially diminishing the contribution of the other parameters.

All indicators are insensitive to both v_{suit} and h_{min} suggesting to set a fix value for them. For v_{suit}, as explained above, this observation may be different if either a larger range for v_{suit} would be sampled or other reaches would be modelled. Similarly, the relevance of λ_{mid} may be larger if its sample range would have been less confined when ensuring

independent sampling (s. Section 2.1.4). The same is true for h_{min} but it would probably only become important for larger fish species since a value of a few centimetres would be within the uncertainty of the hydraulic model (e.g. Juárez et al., 2019). Generally, v_{crit}, Δ_t and λ_{max} affect the indicators the most and effort during parameter estimation should focus on them. Indicator behaviour was overall as expected, i.e. sensitive to parameters influencing their computation directly (e.g. HS_{75}) or through model algorithms (e.g. L_{75}). However, as discussed for v_{suit}, sensitivities might vary with ramping direction and study reach.

The indicators WHL and WCH are the most sophisticated and provide most information. Whereas WHL represents the risk for fish to strand or drift WCH is assessing the persistent suitability of the reach throughout the hydropeaking scenario. With their different focus selection of the most suitable indicator depends on the problem to be addressed. However, they also require the most information making them more laborious to reliably compute. P_d, in contrast to WHL, does not consider the likelihood of fish presence but still gives an estimation of stranding and drifting risk. Similarly, HS_{75} characterises the effect of bed topography on fish escape movement without the need for preference curves. The smallest amount of data is required for L_{75} but it is also the least informative indicator as it ignores the temporal aspect of hydropeaking.

Section 4.2.1 gives a potential reason why the downramping sensitivity analysis failed.

4.1.2. Validation

The side channel falling dry at stranding site *E1* (Figure 15II, more detailed in Figure 16a) forms multiple branches and dead ends throughout the process (dark brown) potentially creating traps for fish. Together with both origin and target habitats close by, increasing the likelihood of fish presence and escape movement through the side channel, a high risk for stranding appears reasonable. Hence, the model is considered to correctly predict the risk at this stranding site although improvements could be made to better highlight it in the result image. Pool formation accompanied by trapping of fish is considered to be the mechanism behind the stranding events observed at site *E2* and *G* (Figure 15II & III, more detailed in Figure 16b) as depressions of the river bottom coincide with physically disconnected origin habitat (Figure 29, Appendix E). Both mechanism are reported to cause stranding at other rivers as well (Larrieu, Pasternack and Schwindt, 2021; Larrieu and Pasternack, 2021). With stranding site *M* (Figure 15IV) not standing out in the model results, stranding risk was correctly visualised at three out of four sites. Although the model indicates other locations of higher risk without reported stranding events its performance is satisfying. Absence of fish, less severe conditions and stranding events not being noticed or reported can be reasons for the apparent type II errors. However, as only one reach and one downramping scenario was tested for only one species the validation is of limited credibility. Apparently the model is capable of reproducing areas of stranding risk but more sophisticated validation is required for a comprehensive conclusion on the model performance.

4.1.3. Limitations

From the sensitivity analysis and the validation several limitations of the model are revealed. First and foremost calculated paths show the optimum behaviour a fish could express. Fine scale fish behaviour is highly complex, understood to only a limited extend and might differ significantly (Pavlov et al., 2008; David and Closs, 2002; Goodwin et al., 2006). Therefore, the model can only provide the best case scenario where a fully-informed fish takes always the best decision for reaching the target habitat. This limitation may explain why the model failed to predict higher risk at stranding site *M*. Nevertheless, the model is capable of determining the theoretical capability of fish to successfully respond to habitat shift. If this theoretical capability does not exist, stranding or drifting of fish is inevitable, thus the model enables evaluation of hydropeaking reaches to a minimum standard. The impact of optimum behaviour on pathway suitability may be approximated by comparing results from optimum and random-walk behaviour. With better understanding of fish behaviour refinement of the model to predict the actual success of fish escape movement during hydropeaking can be achieved.

Secondly, the temporal resolution, i.e. the number of intermediate ΔQ, likely affects the obtained paths. Since the path-finding algorithm computes paths segments for pairs of habitats, they act as a priori defined fixpoints. With more ΔQ more pairs of habitats, i.e. more fixpoints, are provided. Furthermore, finer variations in depth and velocity, affecting valid neighbours and the dynamic exponential function, are represented with smaller step sizes for ΔQ. An extended sensitivity analysis could evaluate the influence the number of ΔQ has on the model results.

Lastly, desirable target values for the model indicators are unknown. Hence, interpretation whether a situation is acceptable is still a challenge. The FiER model can be used to compare scenarios and reaches but additional research is required to estimate their effective suitability for fish with respect to stranding and drifting.

4.2. Model Application

Different river morphologies and their impact on stranding and drifting risk are discussed in Section 4.2.1. How areas of higher risks can be identified is the topic of Section 4.2.2.

4.2.1. Influence of Morphology on Stranding and Drifting Risk

The flow parameters in Table 4 of the studied reaches confirm the hydraulics to be as expected with highest values for depth and velocity in the narrow channel. With groynes keeping the main currents in the middle of the river at low flows velocity reaches the same values as in the channelised reach although more varied due to the slow flow areas at the banks. At high flows variations in depth diminish as banks, groynes and bars become inundated. At both high and low flows the naturally braided reach stays the most varied since it has the most complex morphology and spans the longest river reach.

With lower water depth and velocities, as well as highest variability, the naturally braided reach features the highest HSI for both up- and downramping. Due to the complexity of its morphology it, however, also poses the largest risk for stranding and drifting as is shown by the highest values for P_d, WHL and L_{75} in all and for HS_{75} in the upramping scenario. This is in line with previous studies highlighting the adverse relation between morphological complexity and stranding risk (Nagrodski et al., 2012; Vanzo, Guido and Siviglia, 2015; Lüthy et al., unpub.). Nonetheless, the naturally braided reach still provides the most connected habitat during both up- & downramping. A larger fish population, supported by more habitat being effectively available (WCH), may be more stable although absolute numbers of stranding fish are higher. Furthermore, stranded fish can be an important resource input to the terrestrial ecosystem (Quinn et al., 2009). This gives an indication of a potential net benefit from morphological restoration although impacts from lower pathway suitability on fish populations are not assessed.

Downramping is more severe than upramping especially in the naturally braided, channelised and groynes reach. Stranding, as discussed in Section 4.1.2, appears to be the most plausible cause in the naturally braided reach where flow velocities are lower and depth variations larger. With more regular bed topography in the groynes and channelised reach stranding seems less likely there. Due to higher velocities in the middle of these reaches, and fishes moving towards the rivers centre line during downramping, fish are prone to swim into currents too strong for them leading to drift, i.e. an interrupted path. This is likely overestimated in the model since flow velocities of the higher discharge are considered during both path finding and fish velocity computation to prevent missing values along the water's edge. An indication of this mechanism can be seen in Figure 25 and 26, Appendix C, where a large fraction of origin habitat already shows supercritical velocities. Since origin habitats must have an initial flow velocity $\leq v_{suit}$ per definition it implies that the flow velocity of these cell increases from $\leq v_{suit}$ to $> v_{crit}$ between the lower and the higher discharge of the first ΔQ. This might be the reason why the downramping sensitivity analysis failed. With a lower lateral velocity gradient, due to generally lower flow velocities and a larger river width, this issue is less pronounced in the gravel bars and naturally braided reach but can still overestimate movement costs.

Generally, the defined indicators fulfil the requirements stated in Section 2.1.3. They are *sensitive* to differences in morphology, as can be seen in Table 5, and to the ramping scenario (Δ_t) as well as partly to fish swimming capacities (v_{crit}) during the sensitivity analysis (Figure 14a). Their *relevance* was shown during the validation (Section 3.1.2) since they aggregate the spatially distributed results used there although admittedly not assessed directly. *Consistency* was not systematically evaluated but the varying length of the reaches had no apparent impact on the indicators. However, whether they better factor in the influence of bed topography on the escape route suitability than the commonly used dewatering rate was not assessed. Computation of the dewatering rate based on the depth raster set is feasible, however, a meaningful comparison without

knowing the environmental implications of the model indicator values poses a challenge (s. Section 4.1.3). Although bed topography is not directly involved in the computation it influences the dewatering rate indirectly by altering river hydraulics. Hence, the model is expected to better represent bed topography influence but this is neither shown nor directly obvious.

4.2.2. Identifying Higher Risk Areas in the Storåne River

Segmentation by number of channels divided the river reach into two distinct groups as shown by the difference in their hydraulic characteristics (Table 7). As expected, depth and velocity are higher in the single channel sections (SCS) but less varied. Accordingly, WCH is higher in multiple channel sections (MCS) as is HSI (s. Section 4.2.1). Indicators, however, are in a similar range for both groups, but most of the identified high stranding risk areas are located in MCS. From this it appears that stranding is the main mechanism reducing pathway suitability in MCS while drifiting is more relevant in SCS. A larger drop in P_d and WHL for MCS moving from the downramping to the upramping scenario, where stranding is not an issue as also indicated by longer paths hinting at drift (L_{75}), supports this notion. This is in line with observing higher velocities in single channel sections.

For river management the patch analysis successfully provided locations where stranding risk is expected based on previous events. While effort against stranding can focus on the determined sites drifting is not assessed by it. The river segmentation analysis includes drifting risk but could not identify single sections to focus on. Most insights are gained by combining both methods identifying stranding to be the main risk in MCS and drift in SCS. As both are based on the FiER model they illustrate the value of the model to river management.

5. Further Improvements and Recommendations

The FiER model was extended and its results made more comprehensible with the definition of new indicators. Nevertheless, potential for further improvements remains. Section 5.1 gives recommendations for further development of the model and Section 5.2 on the indicators and for applications.

5.1. Fish Escaping Routes Model

As discussed in Section 4.1.3 not including fish movement behaviour in the path finding limits the model to best case applications. With the complexity of fish behaviour closely modelling their movements seems currently unrealistic in the small-scale 2D framework of the model. However, an approximation could be reached implementing rule sets for movement which, averaged over the entire reach, would reproduce fish escape movement to a satisfying degree. Potential rules include adjustments to the dynamic exponential function to represent actual rather than optimum behaviour and hydraulic triggers for movement start and stop. For rules to be defined a better understanding of fish behaviour on small scales during hydropeaking is a prerequisite. Also, fish could be allowed to compensate movements slower $|\vec{v}_{path}|$ by swimming faster at another part of the path segment rather than strictly considering the path disconnected. Potentially, further hydraulic parameters, e.g. pressure or shear stress, could be included in the model if decisive for fish movement behaviour.

Secondly, the limited validation, as discussed in Section 4.1.2, reduces the models credibility for practical application. An extensive validation of the model needs to investigate both the computed paths and the resulting drifting and stranding rates. A potential setup is to track fish on cameras reconstructing their paths and linking them to local hydraulic conditions. Using information on fin flapping, obtained from the image tracking, movement, drifting and stranding could be distinguished modes determining where fish loose the ability to follow the path. With a validation fitted to the model its performance can more accurately be determined increasing its credibility.

Lastly, there are still issues in the code which need fixing. Most importantly, how raster values are used in the computation of $|\vec{v}_{fish}|$ needs a rework to prevent both missing values beyond the lower discharge water's edge and an overestimation of drifting in downramping scenarios (s. Section 4.2.2). Potential solution are using lower discharge values where available and higher discharge values otherwise or to interpolate in between the two raster. Furthermore, though of less impact, some path segments of dead ends are plotted in the result image leading to paths apparently leading nowhere. Since both code implementation tests were passed successfully, it appears to be a rendering issue not affecting the indicators.

5.2. Indicators

The sensitivity of the indicators was discussed for the upramping scenario in Section 4.1.1 but could not be evaluated conclusively. Besides investigating the sensitivities during downramping, which requires to understand why their analysis failed in this study, their relevance and consistency must be systematically assessed for a comprehensive conclusion on the aptitude of the indicators. Applying the model on several reaches with different characteristics and known stranding and drifting rates, spanning from low to high, would give the required insight in the indicators behaviour. Furthermore, this step could include estimating the desirable range of indicator values. The simplest approach would take the results from natural river reaches without artificial flow alterations as reference values. Indicator values could potentially be related to population stability, if such information is available for the reaches. Otherwise, a population model and the FiER model could be applied in unison to quantify acceptable indicator values. Finally, the tests run to establish target ranges for the dewatering rate (e.g. Tonolla et al., 2017) could either be modelled, if the required raster data is available, or repeated. The latter approach would also be one of the options to compare the currently used indicators with the ones proposed in this work. From this comparison insights into potential deficit of the current indicators can be assessed. New indicators may be defined as well, for instance directly considering $|\vec{v}_{fish}|$ rather than lumping it together into two connectivity categories.

With an improved and validated FiER model the impact of hydropeaking on fish communities can be assessed more precisely leading to more optimised solutions for hydropower plants. Furthermore, options to new applications arise. For instance, modelling the full hydropeaking cycle, i.e. both up- and downramping, would provide insights into effectively available habitats. Coupled with a full- or multi-year hydrograph and progression of life-stages, represented by changes in the corresponding model parameters, it allows assessment of the long-term suitability of hydropeaking reaches, similar to the approach of Wang et al., 2020.

6. Conclusion

The development of the Fish Escaping Routes (FiER) model for rapidly changing flow, started by Lüthy et al., unpub. was successfully continued. An estimation of fish escape route suitability was implemented. The model is now capable of assessing whether and where fish fail during escape movement if expressing optimum behaviour. Indicators were defined to aggregate the spatially distributed results facilitating comparison of reaches and hydraulic scenarios.

During sensitivity analysis the model parameters and indicators were investigated for an upramping scenario. Critical velocity v_{crit}, duration Δ_t and velocity factor λ_{max} proved to be most important, hence should be carefully selected by the modeller. Indicators behaved as expected and react sensitive to the swimming capacity of fish (v_{crit}), the hydraulic scenario (Δ_t) and river morphology. With the Weighted Habitat Loss WHL and the Weighted Connected Habitat WCH two comprehensive indicators are proposed for evaluating escape route suitability and persistent habitat availability. When data scarcity or uncertainty does not allow the computation of WHL and WCH a range of less sophisticated indicators is suggested. For a downramping scenario a validation with observed stranding events showed promising results encouraging further development of the FiER model.

Applying the model to different river reaches, ranging from channelised to naturally braided, the influence of the river morphology on pathway suitability is reflected by the indicators. As in previous studies an adverse effect of more complex morphology on stranding and drifting risk is observed. However, persistent habitat availability increases as well suggesting a net benefit from higher complexity. Using the model areas posing a higher risk for fish stranding can be identified as was shown for the Storåne River enabling river management to focus their efforts effectively.

Both model and indicators require further development before they can be reliably applied in river management and research. Translating indicator values into environmental implications is necessary to apply them beyond comparative analysis. For the model to gain enough credibility for practical application a thorough validation evaluating both indicators and escape routes is a prerequisite. A major limitation of the model is the computation of optimum rather than actual escape routes restricting applications to best case studies. Approaches on how to address the posed improvements were suggested and research into fish movement behaviour on the micro-scale encouraged.

In conclusion, continuing the development of the FiER model for best-case applications appears both feasible and worthwhile. Furthermore, the model forms a promising base to incorporate future advances in understanding fish movement behaviour on the micro-scale.

References

Arvizu, Dan et al. (2011). „Technical Summary“. In: *IPCC Special Report on Renewable Energy Sources and Climate Change Mitigation*. Ed. by O. Edenhofer et al. Cambridge University Press, Cambridge UK and New York, NY, USA.

Auer, Stefan et al. (Jan. 2017). „Effects of river bank heterogeneity and time of day on drift and stranding of juvenile European grayling (Thymallus thymallus L.) caused by hydropeaking“. In: *Science of the Total Environment* 575, pp. 1515–1521. DOI: 10.1016/j.scitotenv.2016.10.029.

Belaud, A. et al. (Jan. 1989). „Probability-of-use curves applied to brown trout (Salmo trutta fario L.) in rivers of southern France“. In: *Regulated Rivers: Research & Management* 3 (1), pp. 321–336. DOI: 10.1002/rrr.3450030130.

Bell, Ethan et al. (Oct. 2008). „Salmonid Fry Stranding Mortality Associated with Daily Water Level Fluctuations in Trail Bridge Reservoir, Oregon“. In: *North American Journal of Fisheries Management* 28 (5), pp. 1515–1528. DOI: 10.1577/m07-026.1.

Berga, Luis (Sept. 2016). „The Role of Hydropower in Climate Change Mitigation and Adaptation: A Review“. In: *Engineering* 2 (3), pp. 313–318. DOI: 10.1016/J.ENG.2016.03.004.

Bieri, M. (2012). „Operation of complex hydropower schemes and its impact on the flow regime in the downstream river system under changing scenarios“. In: *Communications du Laboratoire de Constructions Hydrauliques* 52. Ed. by A. Schleiss.

Bradford, Michael (1997). *AN EXPERIMENTAL STUDY OF STRANDING OF JUVENILE SALMONIDS ON GRAVEL BARS AND IN SIDECHANNELS DURING RAPID FLOW DECREASES*, pp. 395–401.

Bradford, Michael et al. (May 1995). „An Experimental Study of the Stranding of Juvenile Coho Salmon and Rainbow Trout during Rapid Flow Decreases under Winter Conditions“. In: *North American Journal of Fisheries Management* 15 (2), pp. 473–479. DOI: 10.1577/1548-8675(1995)015<0473:AESOTS>2.3.CO;2.

Chan, Gabriel, Robert Stavins and Zou Ji (2018). „International Climate Change Policy“. In: DOI: 10.1146/annurev-resource. URL: https://doi.org/10.1146/annurev-resource-.

Council, The Swiss Federal (Jan. 2021). *Waters Protection Ordinance (WPO)*. URL: https://www.fedlex.admin.ch/eli/cc/1998/2863_2863_2863/en (visited on 18/08/2022).

David, Bruno O. and Gerard P. Closs (July 2002). „Behavior of a Stream-Dwelling Fish before, during, and after High-Discharge Events“. In: *Transactions of the American Fisheries Society* 131 (4). Too low temporal and spatial scale: Twice a day location was determined, i.e. in which pool a fish was located., pp. 762–771. DOI: 10.1577/1548-8659(2002)131<0762:boasdf>2.0.co;2.

ECOHZ (2022). *Hol 1 Urunda hydropower in Norway*. URL: https://www.ecohz.com/hol-1-urunda-hydropower-in-norway (visited on 10/08/2022).

FOEN, Federal Office for the Environement (2022). *Hydrological Atlas of Switzerland*. URL: https://hydrologicalatlas.ch/ (visited on 10/08/2022).

Goodwin, R. Andrew et al. (Feb. 2006). „Forecasting 3-D fish movement behavior using a Eulerian-Lagrangian-agent method (ELAM)“. In: *Ecological Modelling* 192 (1-2). too detailed, as requires 3D information on strains and pressures, pp. 197–223. DOI: 10.1016/j.ecolmodel.2005.08.004.

Greimel, Franz et al. (2018). „Hydropeaking Impacts and Mitigation“. In: *Riverine Ecosystem Management - Science for Governing Towards a Sustainable Future*. Ed. by Jef Huisman. Springer. DOI: https://doi.org/10.1007/978-3-319-73250-3.

Hafslund, ECO AS (2022). *Hol 1*. URL: https://hafslund.no/kraftverk/hol-1@online (visited on 10/08/2022).

Halleraker, J. H. et al. (Sept. 2003). „Factors influencing stranding of wild juvenile brown trout (Salmo trutta) during rapid and frequent flow decreases in an artificial stream“. In: *River Research and Applications* 19 (5-6), pp. 589–603. DOI: 10.1002/rra.752.

Heggenes, J (1988). *Downstream migration and critical water velocities in stream channels for fry of four salmonid species*. Criticical snout velocities of fry brown trout (swim-up, 2weeks, 8weeks) for two different temperatures., pp. 717–727.

Higgins, P and M Bradford (1996). „Evaluation of a Large-Scale Fish Salvage to Reduce the Impacts of Controlled Flow Reduction in a Regulated River“. In: *North American Journal of Fisheries Management* 16 (1), pp. 666–673. DOI: 10.1577/1548-8675(1996)016<0666:EOALSF>2.3.CO;2.

Irvine, Robyn L. et al. (May 2009). „The effects of flow reduction rates on fish stranding in British Columbia, Canada“. In: *River Research and Applications* 25 (4), pp. 405–415. DOI: 10.1002/rra.1172.

Juárez, Ana et al. (Jan. 2019). „Performance of a two-dimensional hydraulic model for the evaluation of stranding areas and characterization of rapid fluctuations in hydropeaking rivers“. In: *Water (Switzerland)* 11 (2). DOI: 10.3390/w11020201.

Kartverket (2022). *Geovekst*. URL: https://www.kartverket.no/en/geodataarbeid/geovekst (visited on 19/08/2022).

Killingtveit, Å̊nund (Nov. 2018). „Hydropower“. In: *Managing Global Warming: An Interface of Technology and Human Issues*. Elsevier, pp. 265–315. ISBN: 9780128141052. DOI: 10.1016/B978-0-12-814104-5.00008-9.

KWO, Kraftwerke Oberhasli AG (2022). *Strom aus Wasserkraft*. URL: https://www.grimselstrom.ch/produktion/strom-aus-wasserkraft/ (visited on 10/08/2022).

Larrieu, Kenneth G. and Gregory B. Pasternack (Sept. 2021). „Automated analysis of lateral river connectivity and fish stranding risks. Part 2: Juvenile Chinook salmon stranding at a river rehabilitation site“. In: *Ecohydrology* 14 (6). DOI: 10.1002/eco.2303.

Larrieu, Kenneth G., Gregory B. Pasternack and Sebastian Schwindt (Mar. 2021). „Automated analysis of lateral river connectivity and fish stranding risks—Part 1: Review, theory and algorithm“. In: *Ecohydrology* 14 (2). DOI: 10.1002/eco.2268.

Lechner, Aaron, Hubert Keckeis and Paul Humphries (Sept. 2016). „Patterns and processes in the drift of early developmental stages of fish in rivers: a review“. In: *Reviews in Fish Biology and Fisheries* 26 (3), pp. 471–489. DOI: 10.1007/s11160-016-9437-y.

Lucas, Martyn et al. (2001). *Migration of Freshwater Fishes*. Oxford: Blackwell Science Ltd. ISBN: 0-632-05754-8.

Lüthy, Elian et al. (2021). *What are the Pathways? A method to assess habitat shifts for larvae during hydropeaking*. Master Tesis, not published. ETH Zurich - Institute for Environmental Engineering.

Melcher, Andreas, Christoph Hauer and Bernhard Zeiringer (2018). „Aquatic Habitat Modeling in Running Waters“. In: *Riverine Ecosystem Management - Science for Governing Towards a Sustainable Future*. Ed. by Jef Huisman. Springer. DOI: https://doi.org/10.1007/978-3-319-73250-3.

Nagrodski, Alexander et al. (July 2012). „Fish stranding in freshwater systems: Sources, consequences, and mitigation“. In: *Journal of Environmental Management* 103, pp. 133–141. DOI: 10.1016/j.jenvman.2012.03.007.

Pathak, M. et al. (2022). „Technical Summary“. In: *Climate Change 2022: Mitigation of Climate Change. Contribution of Working Group III to the Sixth Assessment Report of the Intergovernmental Panel on Climate Change*. Ed. by P.R. Shukla et al. Cambridge University Press, Cambridge UK and New York, NY, USA.

Pavlov, Dmitrii S. et al. (Sept. 2008). „Ecological and behavioural influences on juvenile fish migrations in regulated rivers: A review of experimental and field studies“. In: *Hydrobiologia* 609 (1), pp. 125–138. DOI: 10.1007/s10750-008-9396-y.

QGIS Development Team (2022). *QGIS Desktop 3.22.7*. URL: https://www.qgis.org (visited on 31/05/2022).

Quinn, Thomas P. et al. (2009). „Transportation of Pacific salmon carcasses from streams to riparian forests by bears“. In: *Canadian Journal of Zoology* 87.3, pp. 195–203. DOI: 10.1139/Z09-004.

Roth, Hans Peter (3rd Oct. 2019). „Die teure Bändigung der Hasli-Aare“. In: *Berner Zeitung*. URL: https://www.bernerzeitung.ch/die-teure-baendigung-der-hasli-aare-835822998504?idp=OneLog&new_user=no (visited on 10/08/2022).

Saltelli, Andrea et al. (2008). „Variance-based methods: How to compute sensitivity indices“. In: *Global sensitivity analysis : the primer*. John Wiley & Sons, Ltd. Chap. 4.6, pp. 164–167.

Schweizer, Steffen et al. (Dec. 2013). „Schwall/Sunk-Sanierung in der Hasliaare - Phase 1a: Gewässerökologische Bestandsaufnahme“. In: *Wasser Energie Luft*.

Steffen, Will et al. (Feb. 2015). „Planetary boundaries: Guiding human development on a changing planet“. In: *Science* 347 (6223). DOI: 10.1126/science.1259855.

Tonolla, Diego et al. (2017). *Schwall-Sunk – Massnahmen. Ein Modul der Vollzugshilfe Renaturierung der Gewässer*. Bundesamt für Umwelt, Bern.

Vanzo, Davide, Zolezzi Guido and Annunziato Siviglia (Apr. 2015). *Eco-hydraulic quantification of hydropeaking and thermopeaking: development of modeling and assessment tools*. University of Trento - Department of Civil, Environmental and Mechanical Engineering.

Wang, Li et al. (June 2020). „Incorporating fish habitat requirements of the complete life cycle into ecological flow regime estimation of rivers“. In: *Ecohydrology* 13 (4). DOI: 10.1002/eco.2204.

Zarfl, Christiane et al. (Jan. 2015). „A global boom in hydropower dam construction“. In: *Aquatic Sciences* 77 (1), pp. 161–170. DOI: 10.1007/s00027-014-0377-0.

List of Tables

List of Figures

Appendix

List of appendices

A. Model Validity Tests

To verify that the model behaves as intended two tests were defined. The first one, presented it Figure 18, inspects the path finding algorithm and the fish velocity computation. A simple scenario with one source and one target cell was defined, separated by a barrier (e.g. an emerged gravel bar). Water depth, velocity in x- and y-direction as well as all parameters were identical for the by-hand calculation and for the model. Figure 18b and 18c show the results respectively. As they are identical the vaidity test ist passed by the model.

Similarly, a test was created to verify the indicator computation. It consists of five reaches of identical structure, of which one is split by a barrier (Figure 19a). The reaches differ in terms of water depth and flow velocity as can be seen in different paths and/or maximum fish velocity in Figure 19b (by-hand calculation) and 19c (model). Both the result image as well as the computed indicators (Figure 19d) verify that the code works as intended.

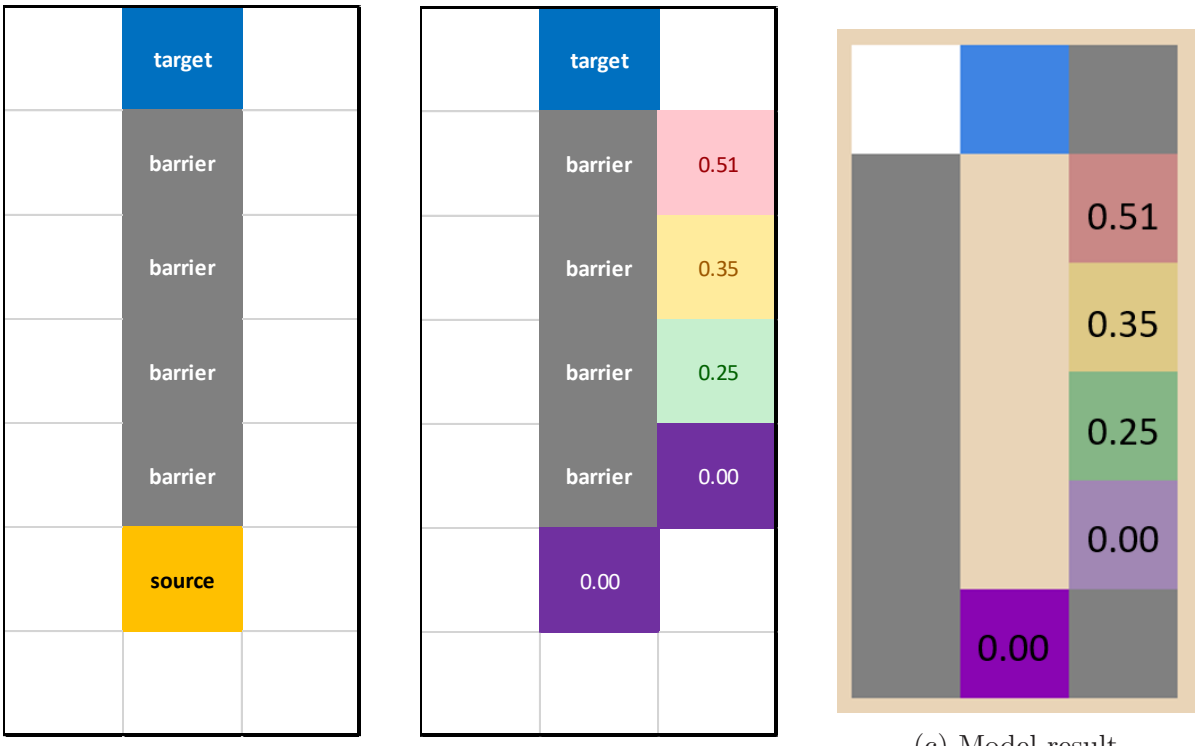

(a) Test setup (b) By-hand result (c) Model result

Figure 18: The test reach for the fish velocity is illustrated in Subfigure (a). Obtained $|\vec{v}_{fish}|$ from calculation by-hand (Subfigure b) and using the model (Subfigure c) are identical, i.e. the code behaves as intended.

(a) Test setup

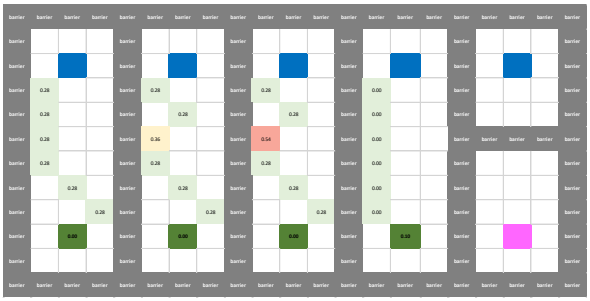

(b) By-hand result

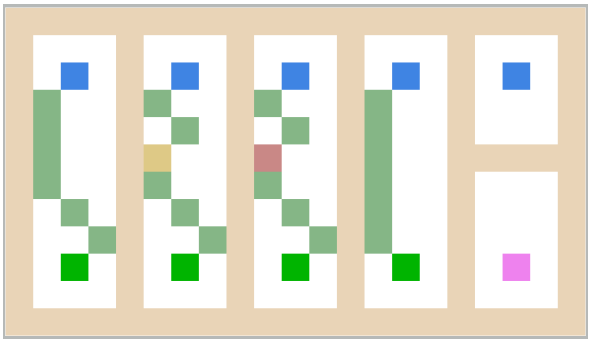

(c) Model result

Indicator	By-hand	Model
P_d	40.00%	40.00%
WHL	41.44%	41.43%
WCH	1.88%	1.88%
L_{75}	2.30 m	2.30 m
HSI_{75}	9.20 $\frac{\text{m}}{\text{h}}$	9.21 $\frac{\text{m}}{\text{h}}$

(d) Indicator values

Figure 19: The test reach for the indicator computation is illustrated in Subfigure (a). Obtained $|\vec{v}_{fish}|$ from calculation by-hand (Subfigure b) and using the model are identical. In Table (d) the respective indicator values are presented. The code behaves as intended.

B. Downramping Sobol Sensitivity Indices

As stated in Section 3.1.1 the obtained Sobol sensitivity indices for the downramping scenario, based on a sample size of $N = 2'000$ violates the plausibility conditions 19, 20 & 21. Hence, they were excluded from the analysis but are shown here in Figure 20 for completeness.

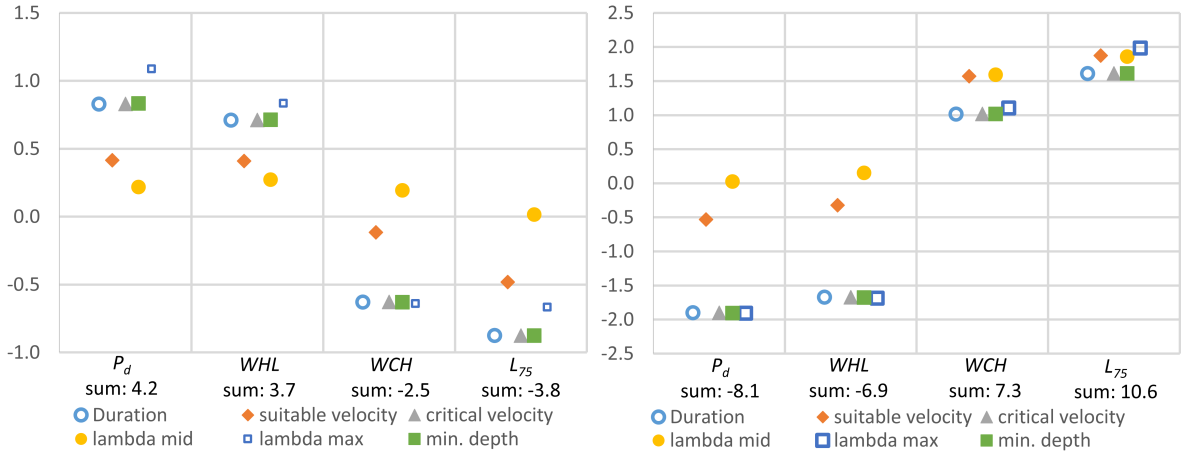

(a) First-order index S_i (b) Total-effect index S_{T_i}

Figure 20: Sobol sensitivity indices for the downramping scenario at the Hasliaare channel reach. Most indicators do not fulfil condition 19, 20 & 21.

C. Result Images of Study Reaches

Figure 21, 22, 23 and 24 show the result images for studied reaches in the upramping scenario. The downramping scneario result images are presented in Figure 25, 26, 27 and 28. For assistance on reading them see Box 3.

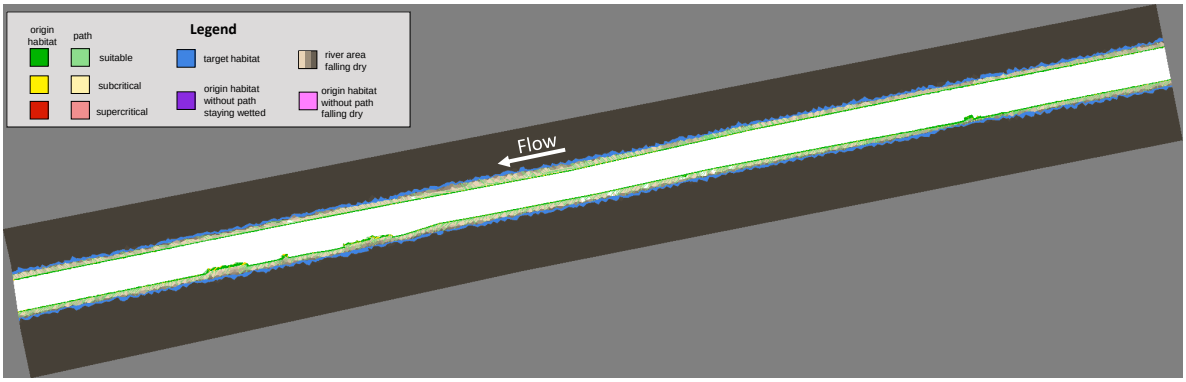

Figure 21: Upramping result image for the channelised reach.

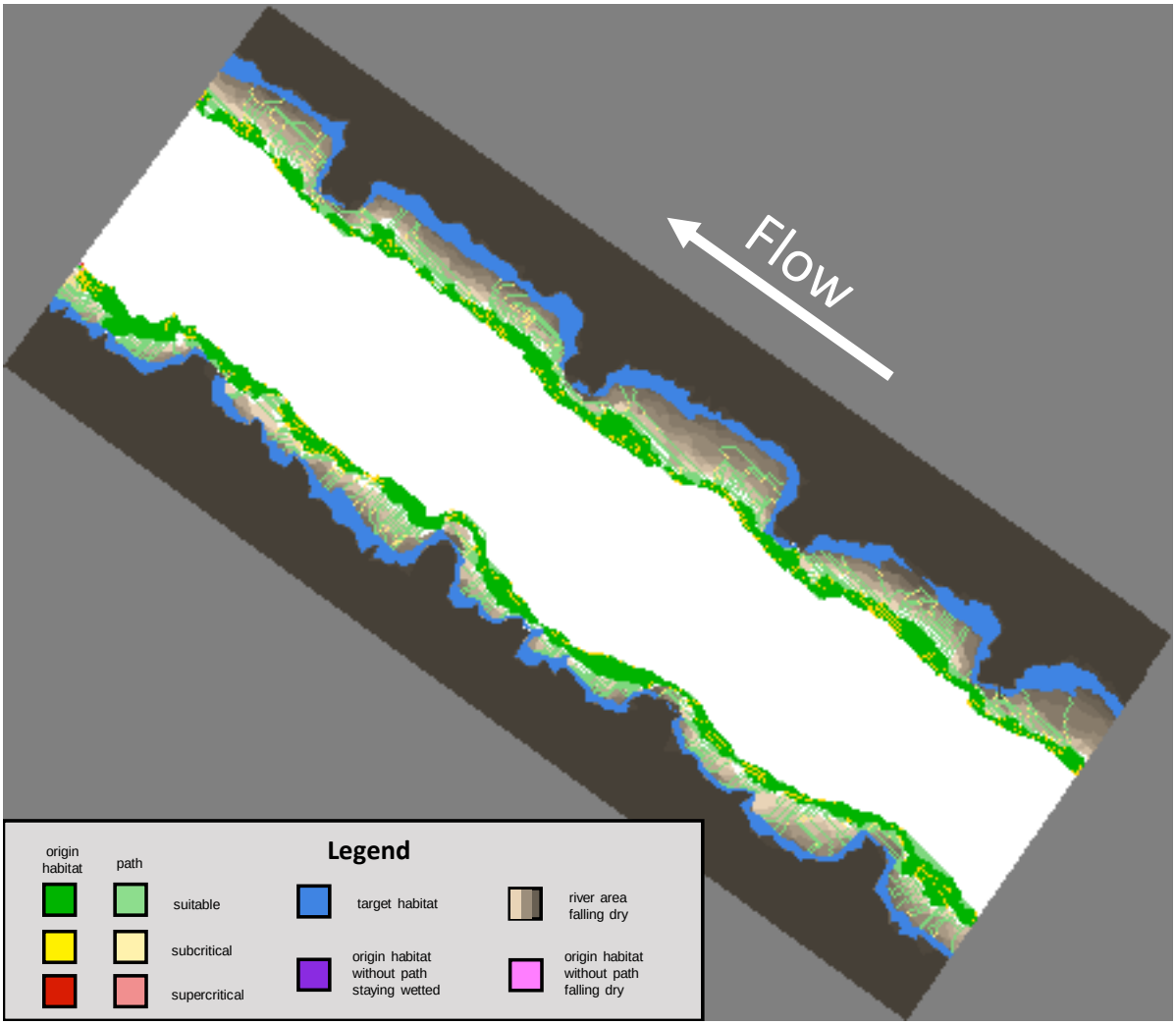

Figure 22: Upramping result image for the groynes reach.

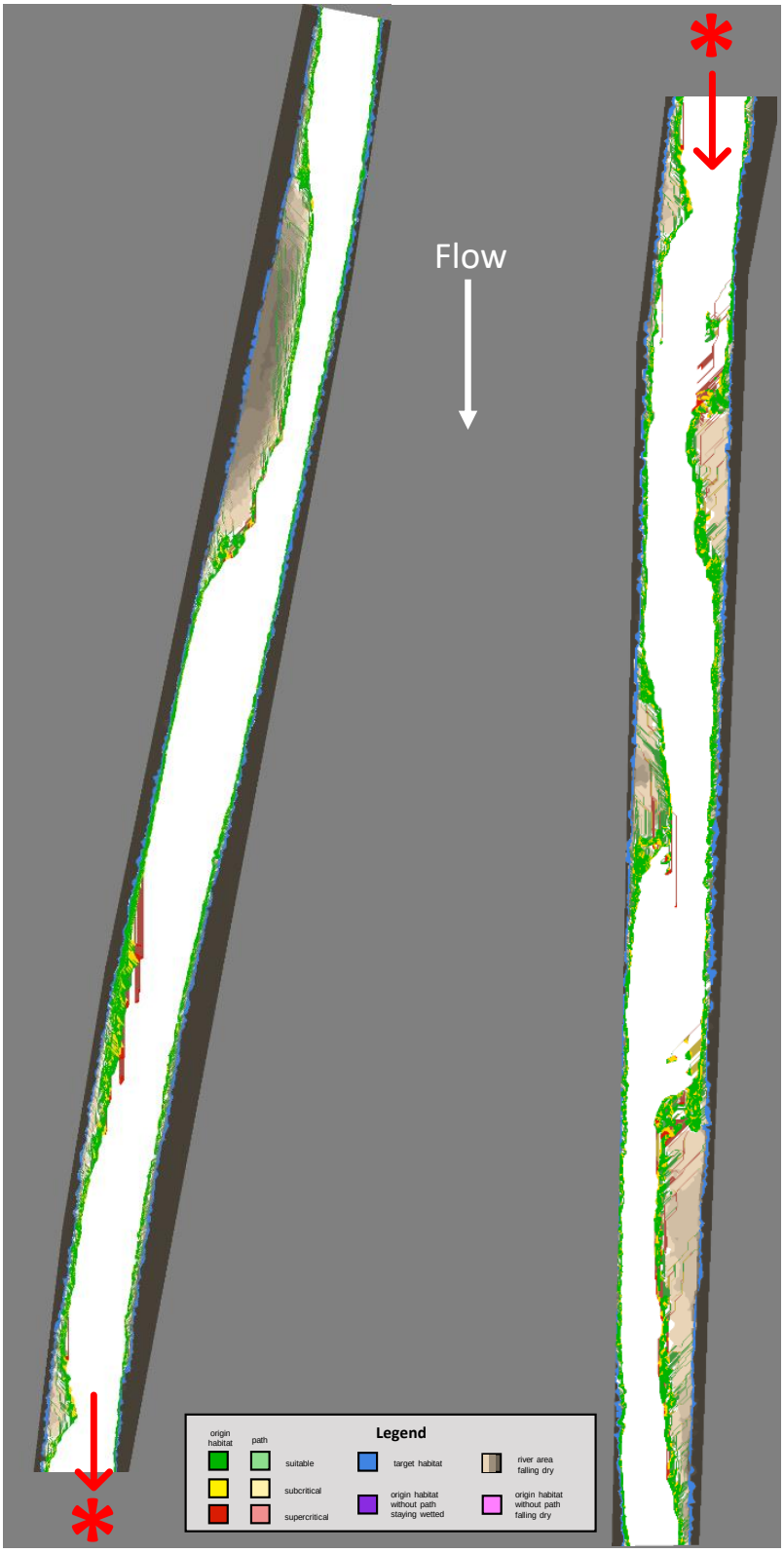

Figure 23: Upramping result image for the gravel bars reach. Split for readability with a small overlap. The left subreach is upstream of the right image.

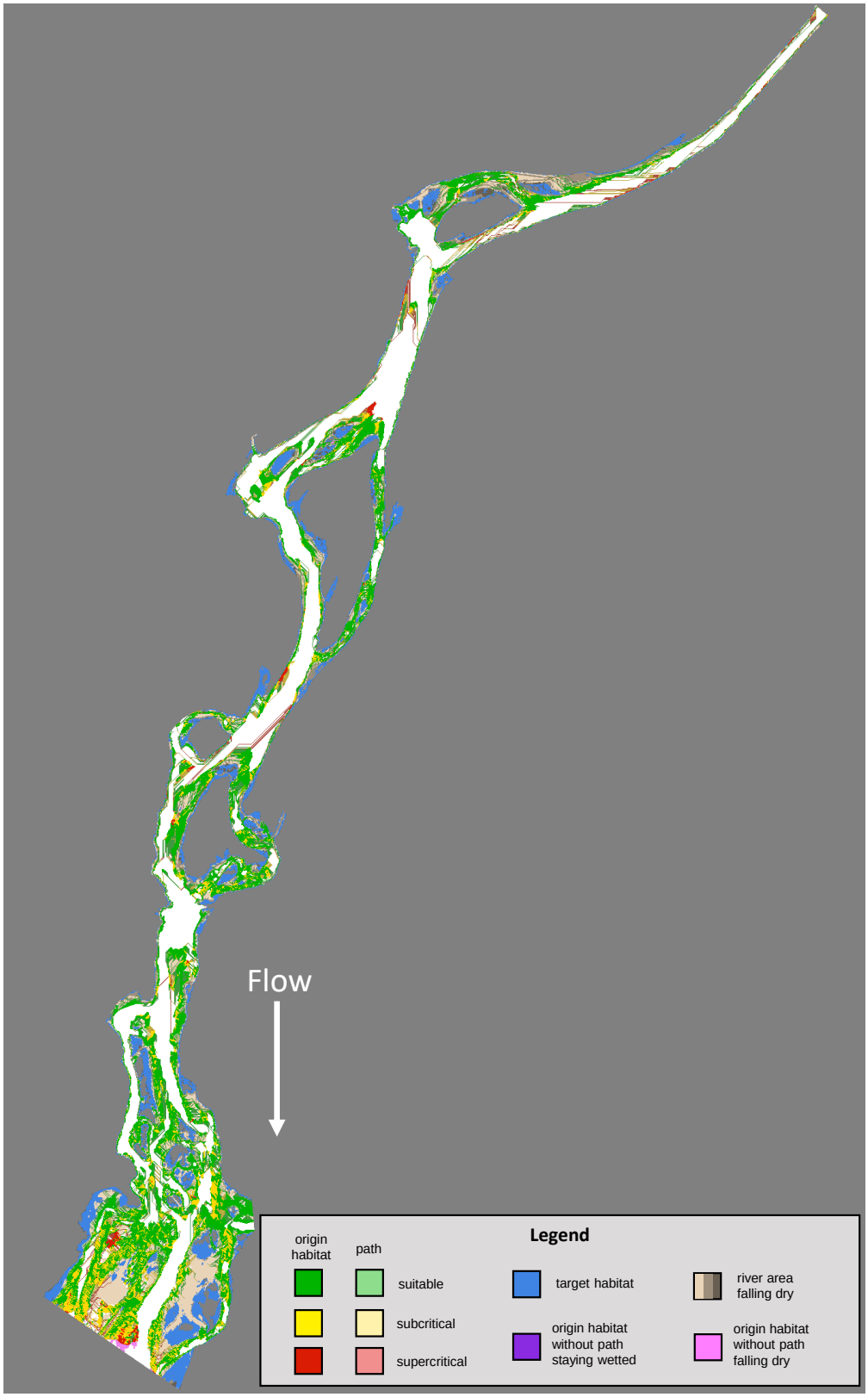

Figure 24: Upramping result image for the naturally braided reach.

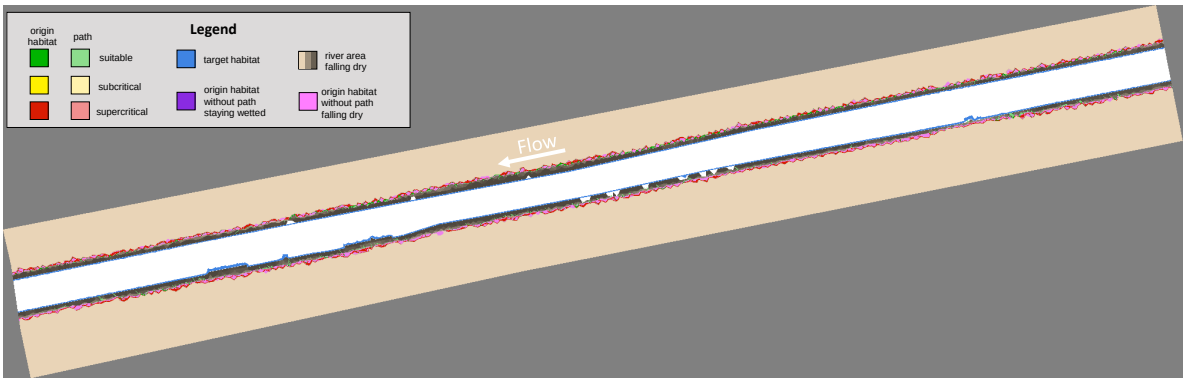

Figure 25: Downramping result image for the channelised reach.

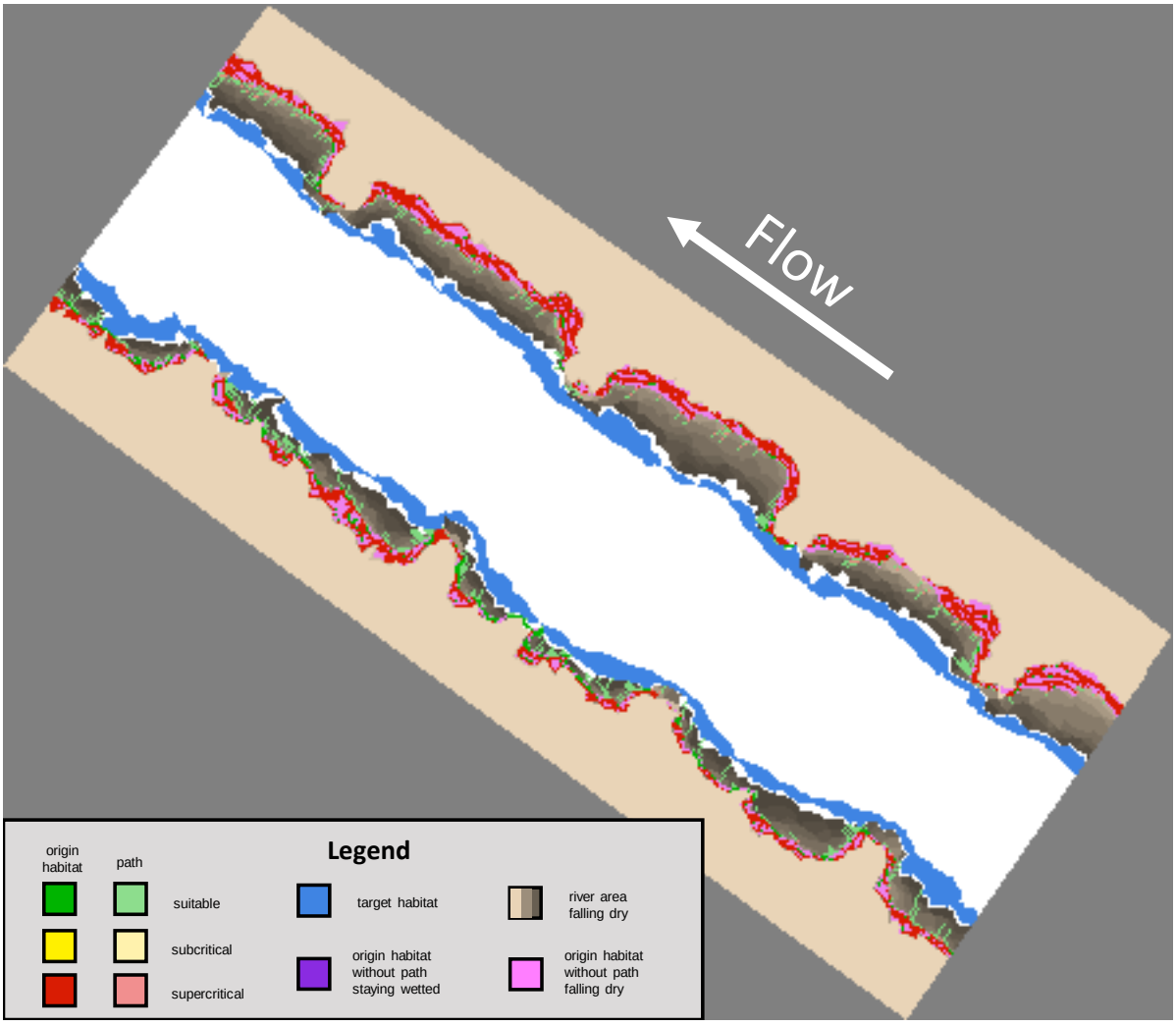

Figure 26: Downramping result image for the groynes reach.

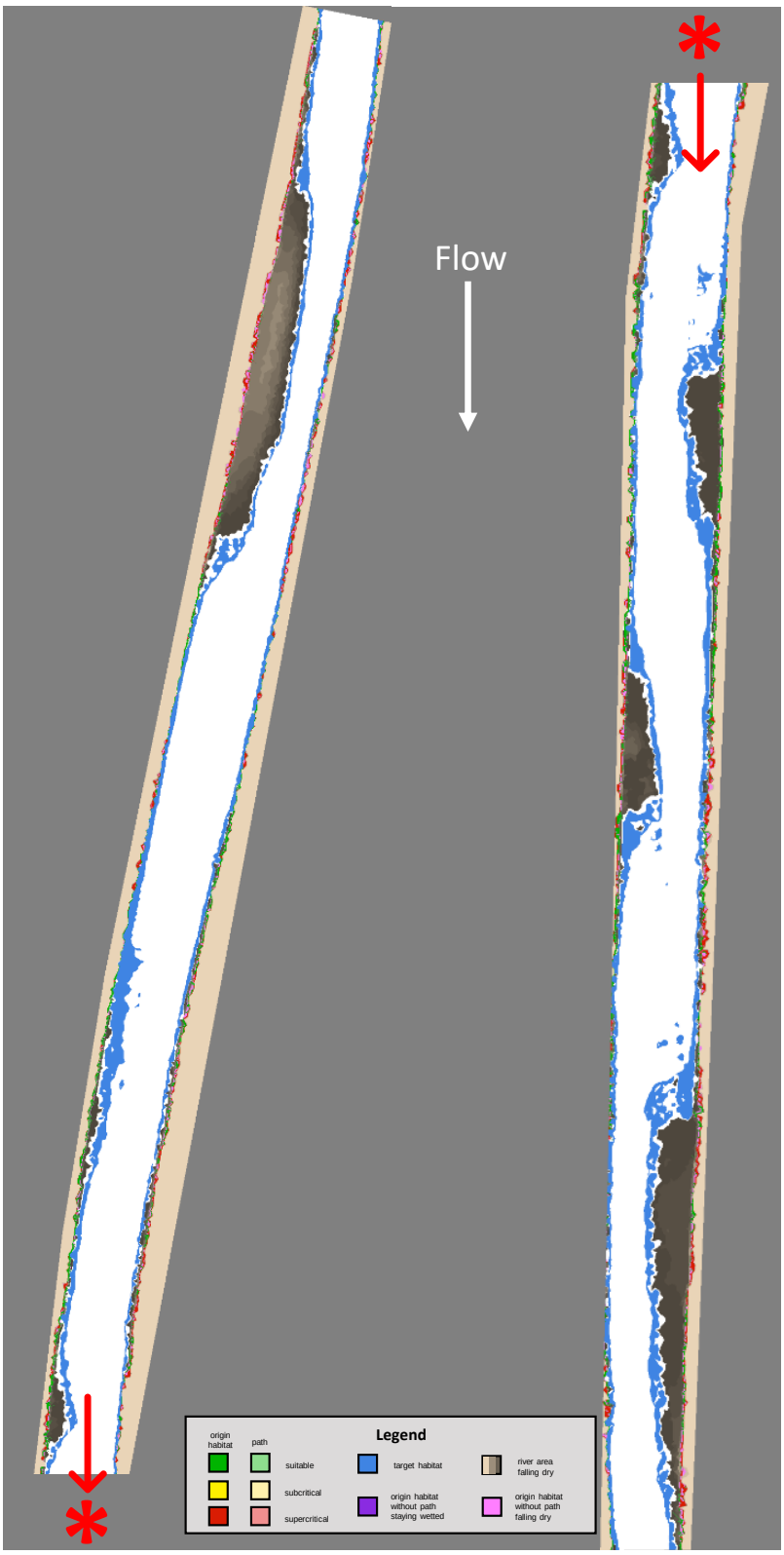

Figure 27: Downramping result image for the gravel bars reach. Split for readability with a small overlap. The left subreach is upstream of the right image.

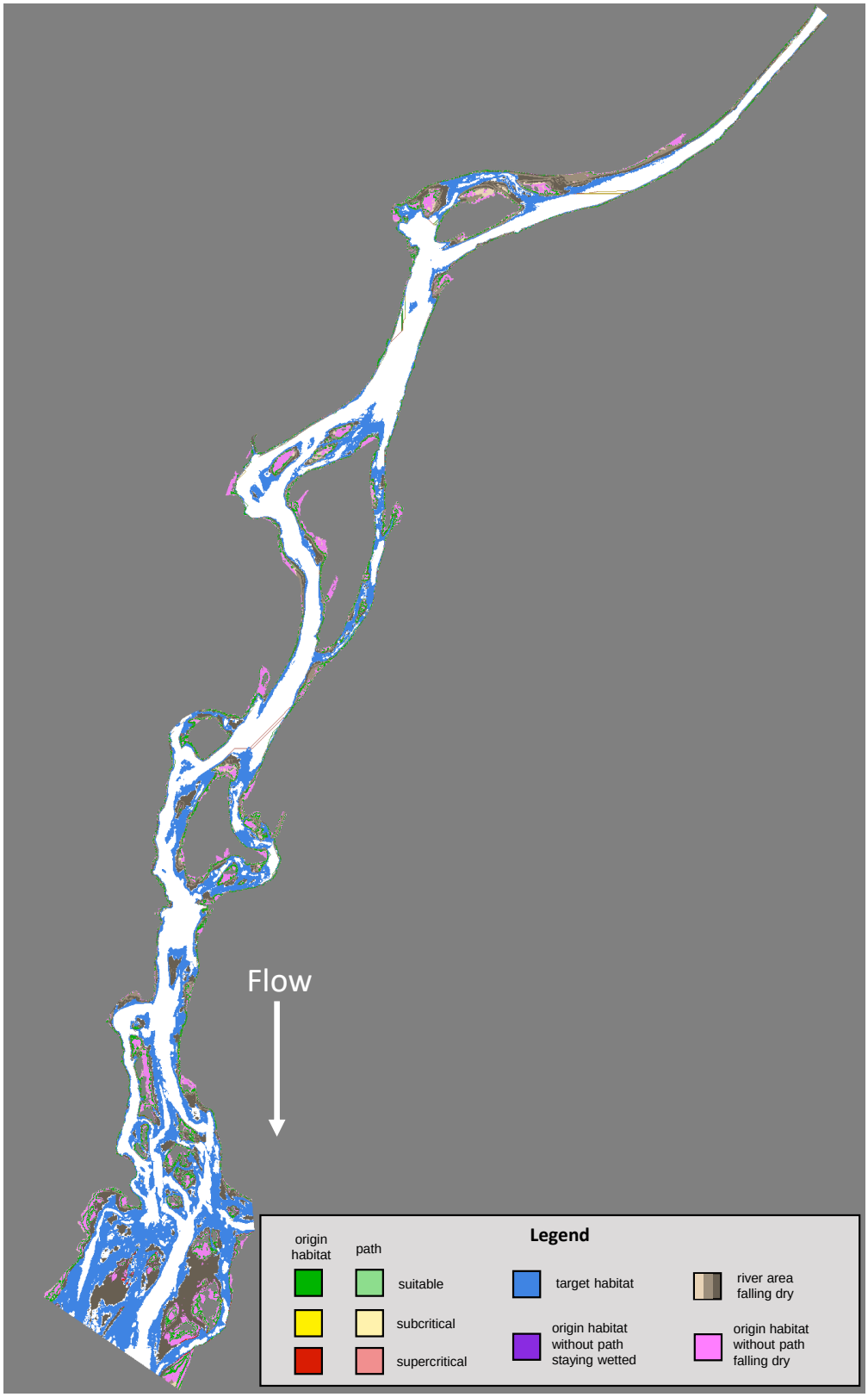

Figure 28: Downramping result image for the naturally braided reach.

D. Detailed Results of River Section Analysis

Section	Unit	1	2	3	4	5	6	7	8	mean	mean	all
Type		single	multiple	single	multiple	single	multiple	single	multiple	single	multiple	
No. risk areas		1	3	0	1	0	3	1	12	0.50	4.75	21
$\mu_{50,h}\ Q^*_{high}$	m	1.39	0.81	1.41	0.80	1.16	0.86	1.14	0.54	1.28	0.75	0.75
$\sigma_h\ Q^*_{high}$	m	0.59	0.74	0.41	0.76	0.60	1.10	0.87	0.39	0.62	0.75	0.72
CV_h	–	42.4%	91.4%	29.1%	95.0%	51.7%	127.9%	76.3%	72.2%	48.4%	99.3%	96.0%
$\mu_{50,v}\ Q^*_{high}$	$\frac{m}{s}$	1.18	0.72	0.66	0.61	0.73	0.55	0.61	0.43	0.80	0.58	0.54
$\sigma_v\ Q^*_{high}$	$\frac{m}{s}$	0.52	0.47	0.18	0.40	0.33	0.33	0.25	0.22	0.32	0.36	0.38
CV_v	–	44.1%	65.3%	27.3%	65.6%	45.2%	60.0%	41.0%	51.2%	40.3%	61.5%	70.4%
WA*** Q^*_{high}	m^2	15'057	24'089	11'435	37'244	7'373	35'771	8'349	100'835	10'554	49'485	240'153
$WUA\ Q^*_{high}$	m^2	906	2'848	584	5'377	1'065	4'380	360	11'963	654	6'142	27'183
$HSI\ Q^*_{high}$	–	6.2%	11.8%	2.5%	14.4%	14.4%	12.2%	4.3%	11.9%	6.9%	12.6%	11.3%
P_d	–	55.6%	62.0%	13.4%	57.8%	65.4%	48.9%	47.7%	59.2%	45.5%	57.0%	57.0%
WHL	–	55.6%	60.8%	13.3%	57.1%	66.2%	47.8%	47.7%	58.3%	45.7%	56.0%	56.2%
WCH	–	2.7%	4.6%	2.2%	6.2%	4.9%	6.4%	2.3%	5.0%	3.0%	5.5%	5.0%
L_{75}	m	8.91	3.83	4.87	3.84	2.84	3.86	3.85	2.83	5.12	3.59	3.51
HS_{75}	m	36.24	36.15	36.05	36.07	0.00	36.02	36.00	0.00	27.07	27.06	35.98
WA Q^{**}_{low}	m^2	13'303	20'612	11'193	33'994	6'032	32'257	7'840	93'912	9'592	45'194	219'150
$WUA\ Q^{**}_{low}$	m^2	1'483	4'457	729	8'864	850	9'648	1'895	34'631	1'239	14'400	62'557
$HSI\ Q^{**}_{low}$	–	11.2%	21.6%	6.5%	26.1%	14.1%	29.9%	24.2%	36.9%	14.0%	28.6%	28.6%
P_d	–	33.5%	35.3%	44.7%	27.2%	23.2%	23.6%	38.4%	25.3%	34.9%	27.9%	26.7%
WHL	–	33.2%	34.3%	44.4%	26.2%	24.0%	22.9%	37.8%	24.5%	34.8%	27.0%	25.9%
WCH	–	7.5%	14.2%	3.6%	19.3%	10.7%	23.1%	15.1%	27.8%	9.2%	21.1%	21.2%
L_{75}	m	38.78	50.79	68.79	37.2	25.99	54.07	67.69	40.61	50.31	45.67	43.7
HS_{75}	m	412.01	554.54	189.00	377.47	392.25	407.52	455.39	254.41	362.16	398.49	333.01

* Q_{high} describes a discharge of 51 $\frac{m^3}{s}$ ** Q_{low} describes a discharge of 6 $\frac{m^3}{s}$ *** WA: Wetted Area

Table 9: Hydraulic (upper), downramping (middle), and upramping (lower) indicators for the section-wise calculation of the naturally braided reach. Also shown are the means for single and multiple channel sections and results from modelling the entire reach.

E. Water Depth at Pool Type Stranding Sites

Figure 29 shows the water depths for 51 $\frac{m^3}{s}$, i.e. depth of the first input raster set during the validation (Section 4.1.2), at the sites where pool stranding was observed. Isolated patches of deeper water depth indicate pool formation.

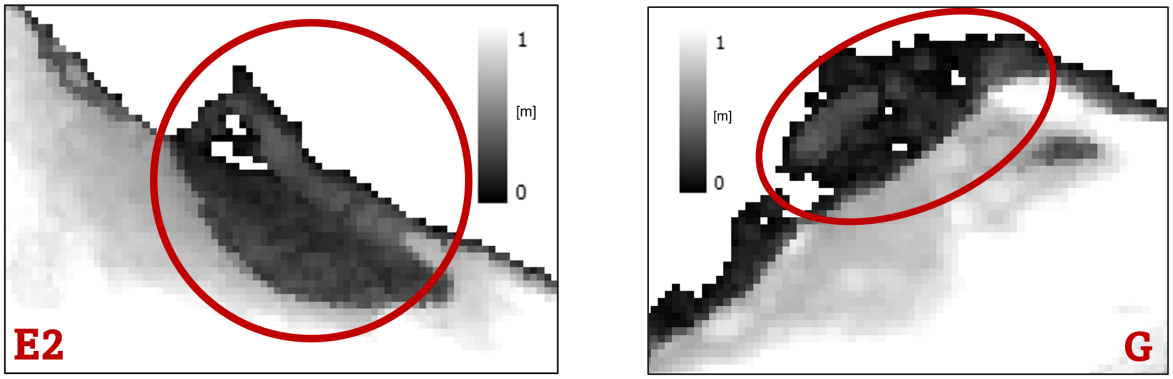

(a) Stranding site E2

(b) Stranding site G

Figure 29: Water depth showing the depression at stranding site E2 and G causing pool type stranding.

F. Declaration of Originality

Eidgenössische Technische Hochschule Zürich
Swiss Federal Institute of Technology Zurich

Declaration of originality

The signed declaration of originality is a component of every semester paper, Bachelor's thesis, Master's thesis and any other degree paper undertaken during the course of studies, including the respective electronic versions.

Lecturers may also require a declaration of originality for other written papers compiled for their courses.

I hereby confirm that I am the sole author of the written work here enclosed and that I have compiled it in my own words. Parts excepted are corrections of form and content by the supervisor.

Title of work (in block letters):

Quantifying Pathway Suitability for Fish Escaping Rapid Flow Changes

Authored by (in block letters):
For papers written by groups the names of all authors are required.

Name(s):	**First name(s):**
Wittmann	Joël Ronald

With my signature I confirm that
- I have committed none of the forms of plagiarism described in the 'Citation etiquette' information sheet.
- I have documented all methods, data and processes truthfully.
- I have not manipulated any data.
- I have mentioned all persons who were significant facilitators of the work.

I am aware that the work may be screened electronically for plagiarism.

Place, date	**Signature(s)**
Zurich, 09.09.2022	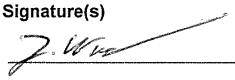

For papers written by groups the names of all authors are required. Their signatures collectively guarantee the entire content of the written paper.